3

Interaction of electromagnetic radiation with matter

The interaction of electromagnetic radiation with matter is evidently fundamental to remote sensing. The subject is a vast one, embracing many areas of physics, and a fully systematic treatment would require at least a book in itself. In this chapter, therefore, we will attempt to provide an overview that will be sufficient to gain an understanding of the operation of remote sensing systems. In order to keep the chapter to a manageable length, we reserve a discussion of the interaction of electromagnetic radiation with the Earth's atmosphere to chapter 4. Nevertheless, this is still a long chapter, and it is also the most technical in the book. It is not necessary to understand all of the material in this chapter in order to follow the subsequent material.

3.1 Propagation through homogeneous materials

To describe propagation in a uniform homogeneous material, we need to introduce two properties of the medium: its *relative electric permittivity* ε_r and its *relative magnetic permeability* μ_r. The relative electric permittivity, which is also known as the *dielectric constant*, is the ratio of ε, the electric permittivity of the material, to ε_0, the permittivity of free space; and the relative magnetic permeability is the ratio of μ, the magnetic permeability μ_0, to the permeability of free space. Thus, we can put

$$\mu = \mu_r \mu_0 \tag{3.1}$$

and

$$\varepsilon = \varepsilon_r \varepsilon_0 \tag{3.2}$$

Both ε_r and μ_r are pure numbers; that is, they are dimensionless. Note that some authors use the symbols ε and μ to represent the relative, rather than the absolute, values of the permittivity and the permeability.

An electromagnetic wave can propagate in such a medium. For consistency with chapter 2, we will write the equation for the electric field in exactly the same form as for the free-space wave defined in equation (2.1):

$$E_x = E_0 \cos(\omega t - kz) \tag{3.3}$$

However, the equation for the magnetic field now differs from equation (2.2), becoming

$$B_y = \frac{E_0\sqrt{\varepsilon_r\mu_r}}{c}\cos(\omega t - kz) \tag{3.4}$$

The ratio of the amplitudes of the electric and magnetic fields has become

$$\frac{c}{\sqrt{\varepsilon_r\mu_r}}$$

instead of c as it is for an electromagnetic wave propagating in free space.

In order for equations (3.3) and (3.4) to represent a valid solution of Maxwell's equations, the angular frequency ω and the wave number k must be related by

$$\frac{\omega}{k} = \frac{c}{\sqrt{\varepsilon_r\mu_r}} \tag{3.5}$$

This is the wave speed, or more precisely the *phase velocity* of the wave (see section 3.1.3), which we denote by the symbol v. The *refractive index* n of the medium is defined as c/v; thus,

$$n = \sqrt{\varepsilon_r\mu_r} \tag{3.6}$$

Clearly, free-space propagation is the special case $n = 1$.

Most of the discussion of polarisation presented in chapter 2 can be applied equally well to the case of a medium in which the refractive index n is not equal to 1. The electric and magnetic fields are still perpendicular to one another and to the direction of propagation, though of course the ratio of the amplitudes is now v rather than c. The Stokes parameters are still defined by equations (2.13). However, the flux density of the radiation (the power transmitted per unit area normal to the propagation direction) is

$$F = \frac{S_0}{2Z} \tag{3.7}$$

where Z, the impedance of the medium, is given by

$$Z = Z_0\sqrt{\frac{\mu_r}{\varepsilon_r}} \tag{3.8}$$

3.1.1 Complex dielectric constants: absorption

We have seen how the behaviour of an electromagnetic wave in a uniform homogeneous medium is controlled by the refractive index n, defined by equation (3.6). For most of the media we shall need to consider, the relative magnetic permeability μ_r can be taken as 1 (these are so-called 'non-magnetic materials'), and we can therefore focus our attention on the dielectric constant ε_r.

For the case of a uniform homogeneous medium that does not absorb any energy from an electromagnetic wave propagating through it, the dielectric constant must be a real number. However, if the medium does absorb energy

from the wave, we must use a complex number to represent the dielectric constant. The conventional way of doing this is to put

$$\varepsilon_r = \varepsilon' - i\varepsilon'' \tag{3.9}$$

where $i^2 = -1$ and ε' and ε'', respectively, are referred to as the real and imaginary parts of the dielectric constant. (Strictly speaking, ε'' is the negative of the imaginary part.) Another commonly encountered way of writing the complex dielectric constant is to put

$$\varepsilon_r = \varepsilon'(1 - i \tan \delta) \tag{3.10}$$

where $\tan \delta$ is called the *loss tangent*. This notation is clearly equivalent to equation (3.9), and is also equivalent to making the refractive index complex (we are still assuming that $\mu_r = 1$):

$$n = m - i\kappa \tag{3.11}$$

which we can see as follows. From equation (3.6), and taking $\mu_r = 1$, we know that

$$n^2 = \varepsilon_r$$

Squaring equation (3.11), and equating it to equation (3.9), gives

$$n^2 = m^2 - \kappa^2 - 2im\kappa = \varepsilon' - i\varepsilon''$$

and so the two descriptions are equivalent provided that

$$\varepsilon' = m^2 - \kappa^2 \tag{3.12.1}$$

$$\varepsilon'' = 2m\kappa \tag{3.12.2}$$

We can also see how a complex dielectric constant represents propagation with absorption by considering an x-polarised wave propagating in the z-direction. The electric field can be written using the complex exponential notation

$$E_x = E_0 \exp(i[\omega t - kz]) \tag{3.13}$$

where E_0 is a constant. This is equivalent to equation (3.3). From equations (3.5) and (3.6) we know that

$$k = \frac{\omega n}{c}$$

which can be rewritten using equation (3.11) as

$$k = \frac{\omega}{c}(m - i\kappa)$$

Substituting this expression for k into equation (3.13), and rearranging, we obtain

$$E_x = E_0 \exp\left(-\frac{\omega\kappa z}{c}\right) \exp\left(i\left[\omega t - \frac{\omega m z}{c}\right]\right)$$

This clearly represents a simple harmonic wave whose amplitude decreases exponentially with the distance z. Since we are usually more interested in the

flux density F of the wave, and this is proportional to the square of the amplitude, we can put

$$F = F_0 \exp\left(-2\frac{\omega\kappa z}{c}\right) \tag{3.14}$$

where F_0 is a constant.

Equation (3.14) shows that the flux density of the electromagnetic wave is reduced by a factor of $e\,(\approx 2.718)$ as the wave advances a distance l_a through the medium, where l_a, the *absorption length*, is given by

$$l_a = \frac{c}{2\omega\kappa} \tag{3.15}$$

If there are no other factors influencing the intensity of the radiation (i.e. we can ignore scattering and emission for the present – although we will discuss these phenomena in section 3.4), the absorption length provides an order-of-magnitude estimate for the distance that radiation will propagate through the material before its intensity is significantly reduced. For example, after travelling two absorption lengths, the intensity is reduced by a factor of e^2, which means that it has been reduced to about 14% of its original value. After five absorption lengths, the intensity is only 0.7% of its original value, and so on. Figure 3.1 shows the variation with frequency of the absorption length in various materials.

3.1.2 Dielectric constants and refractive indices of real materials

The dielectric constant of a real material is normally dependent on the frequency, and the variation can be quite complicated (e.g. see Feynman et al., 1964, volume 2, for a very clear discussion of the physical principles that determine the dielectric constants of real materials). However, over a limited frequency range a simple physical model can often give a satisfactory description. Although the foregoing theory has been developed in terms of the angular frequency ω, it is more usual to specify the frequency f, or, especially for optical and infrared radiation, the *free-space wavelength* λ_0. This is the wavelength that electromagnetic radiation of the same frequency would have if it were propagating in free space, and is given by equations (2.4) and (2.6) as

$$\lambda_0 = \frac{2\pi c}{\omega} = \frac{c}{f} \tag{3.16}$$

The wavelength of the radiation in the medium is given by

$$\lambda = \frac{\lambda_0}{m} \tag{3.17}$$

3.1.2.1 Gases

The dielectric constant of a gas is given to reasonable accuracy, provided that the radiation is not strongly absorbed by the gas, by

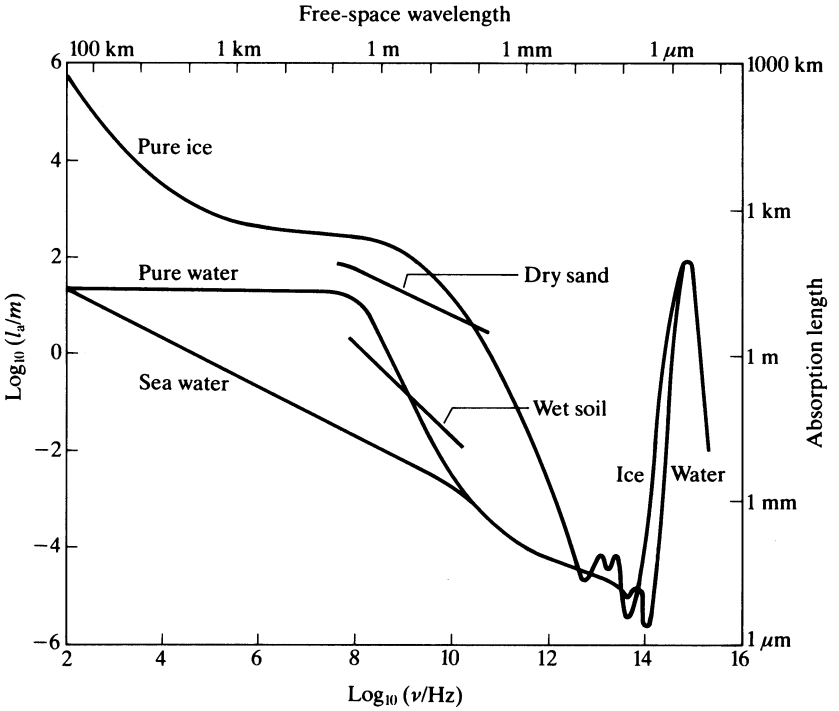

Figure 3.1. Absorption lengths (schematic) of various materials. Note that the absorption lengths are strongly influenced by such factors as temperature and the content of trace impurities, especially at low frequencies.

$$\varepsilon_r = 1 + \frac{N\alpha}{\varepsilon_0} \tag{3.18}$$

where N is the number density of the gas molecules (i.e. the number of molecules per unit volume) and α is the *polarisability* of the gas molecule. Since the term $N\alpha/\varepsilon_0$ is much smaller than 1 for a gas, the refractive index is given, to a good approximation, by

$$n = 1 + \frac{N\alpha}{2\varepsilon_0} \tag{3.19}$$

The quantity α/ε_0 has the dimensions of a volume, and is normally similar to the actual physical volume of the molecule. Table 3.1 shows typical values of this quantity for various gases at optical ($\lambda_0 = 589\,\text{nm}$) and radio (typically 1 MHz) frequencies.

3.1.2.2 Solids and liquids that are electrical insulators

Simple *non-polar* materials are characterised by a constant (possibly complex) value of ε_r. Simple *polar* materials can be described by the *Debye equations* (3.20), which represent a resonant phenomenon with a time-constant (relaxation time) τ:

Table 3.1. Values of α/ε_0 (where α is the molecular polarisability) of various gases at optical and radio frequencies

The values are given in units of 10^{-30} m^3

Gas	Optical	Radio
Air	21.7	21.4
Carbon dioxide	33.6	36.8
Hydrogen	9.8	10.1
Oxygen	20.2	19.8
Water vapour	18.9	368

$$\varepsilon' = \varepsilon_\infty + \frac{\varepsilon_p}{1+\omega^2\tau^2} \tag{3.20.1}$$

$$\varepsilon'' = \frac{\omega\tau\varepsilon_p}{1+\omega^2\tau^2} \tag{3.20.2}$$

In these equations, ε_∞ is the dielectric constant at 'infinite' frequency (in practice, at frequencies much greater than $1/\tau$), and ε_p is the polar contribution to the dielectric constant. For example, pure water follows the Debye equations fairly closely between 1 MHz and 1000 GHz, with values (at 20°C) of $\varepsilon_\infty = 5.0$, $\varepsilon_p = 75.4$, $\tau = 9.2 \times 10^{-12}$ s. The corresponding variation of ε' and ε'' is shown in figure 3.2.

3.1.2.3 Metals

The electrical properties of metals are dominated by the very high densities of delocalised electrons. In general, the dielectric constant of a metal can be written as

$$\varepsilon' = 1 - \frac{\sigma\tau}{\varepsilon_0(1+\omega^2\tau^2)} \tag{3.21.1}$$

$$\varepsilon'' = \frac{\sigma}{\varepsilon_0\omega(1+\omega^2\tau^2)} \tag{3.21.2}$$

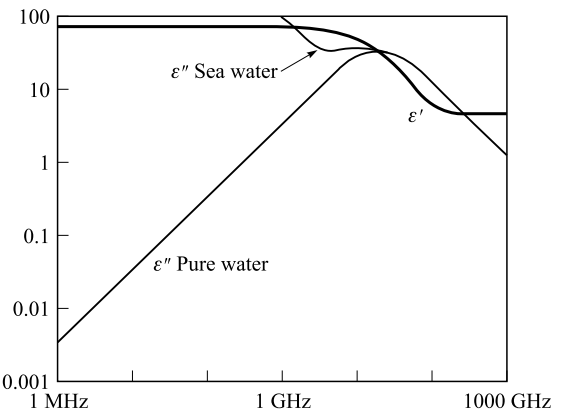

Figure 3.2. Real and imaginary parts of the dielectric constants of pure water and sea water.

In these expressions, σ is the electrical *conductivity* of the metal, and

$$\tau = \frac{m_e \sigma}{Ne^2} \tag{3.22}$$

where m_e is the mass of the electron, e is the charge on the electron, and N is the number density of delocalised electrons in the metal. Equations (3.21) can be simplified for the cases where $\omega \gg 1/\tau$ and where $\omega \ll 1/\tau$. For metals, τ has a value of typically 10^{-15} to 10^{-14} s, so these cases correspond to radio frequencies and optical or ultraviolet frequencies, respectively. At low (radio) frequencies, we obtain

$$\varepsilon_r \approx -\frac{i\sigma}{\varepsilon_0 \omega} \tag{3.23}$$

From equations (3.12) we see that this corresponds to real and imaginary components of the refractive index of

$$m = \kappa = \sqrt{\frac{\sigma}{2\varepsilon_0 \omega}}$$

and hence from equation (3.15) the absorption length is given by

$$l_a = c\sqrt{\frac{\varepsilon_0}{2\sigma\omega}}$$

For example, let us consider electromagnetic radiation at a frequency of 5 GHz ($\omega = 3.14 \times 10^{10}\,\mathrm{s}^{-1}$) propagating in stainless steel ($\sigma = 1.0 \times 10^6\,\Omega^{-1}\,\mathrm{m}^{-1}$). We find that the absorption length is 3.6 μm, which shows that the material is opaque to radio frequency radiation unless it is extremely thin.

At high (optical or ultraviolet) frequencies, the dielectric constant of a metal can be approximated as

$$\varepsilon_r \approx 1 - \frac{Ne^2}{\varepsilon_0 m_e \omega^2} \tag{3.24}$$

which is real and very slightly less than 1. Thus, at sufficiently high frequencies, metals become transparent.

Equation (3.24) also describes the dielectric constant of a *plasma*, a state of matter in which all the atoms have been ionized. Because the mass of the electron is so much smaller than that of any other charged particle, the latter may effectively be ignored in considering the response of the material to an electromagnetic wave. It is clear from equation (3.24) that a plasma is transparent (ε_r is real) for angular frequencies higher than

$$\omega_p = \sqrt{\frac{Ne^2}{\varepsilon_0 m_e}} \tag{3.25}$$

and absorbs radiation at angular frequencies below this value. ω_p is called the *plasma frequency*, and considerations of the properties of plasmas will be important when we discuss the ionosphere.

3.1.3 Dispersion

We noted earlier that, in a number of cases of practical importance, the dielectric properties (and hence refractive index) of a medium vary with frequency. Such media are said to be *dispersive*, and a wave propagating in such a medium is called a *dispersive wave*. It is usual to characterise this behaviour by expressing the angular frequency ω as a function of the wavenumber k, and this relationship is called the *dispersion relation*.

We saw in equation (3.5) that the wave velocity v is given by

$$v = \frac{\omega}{k} \tag{3.26}$$

This is true even if ω varies with k, and v (the wave velocity or *phase velocity*) is the speed at which the crests and troughs of the wave move in the propagation direction. However, if we modulate the wave in some way, for example by breaking it up into pulses, it is this modulation that carries information, and we therefore need to know the speed at which the modulating function travels. This is called the *group velocity*, and it is given by

$$v_g = \frac{d\omega}{dk} \tag{3.27}$$

Only in the case of a non-dispersive wave, for which ω is proportional to k, will equations (3.26) and (3.27) be, in general, equal to one another.

Figure 3.3 illustrates the idea of a dispersive wave. It shows a sinusoidal wave that has been modulated by a Gaussian envelope to give a pulse. The pulse is travelling to the right, and is shown at four equally spaced intervals of time. The circle drawn on each position of the pulse shows the progress of a particular crest of the wave, and it can be seen that this crest is travelling more slowly than the envelope itself. Thus, in this particular case, the phase velocity is less than the group velocity. Figure 3.3 also illustrates another consequence of a wave travelling in a dispersive medium, namely the spreading (elongation) of the envelope as time progresses. Whether this phenomenon occurs depends on the precise form of the dispersion relation.

It will sometimes happen in practice that data about the dispersion relation for a particular medium will be given not as $\omega(k)$, but as $n(\lambda_0)$, the dependence of the refractive index on the free-space wavelength. In this case, equation (3.27) may conveniently be expressed as

$$\frac{c}{v_g} = n - \lambda_0 \frac{dn}{d\lambda_0} \tag{3.28}$$

As an example, we can consider the dispersion of visible light in air. In the optical region, the refractive index of dry air at atmospheric pressure and 15°C can be approximated as

$$n = 1 + \frac{1}{a + b/\lambda_0^2}$$

where $a = 3669$ and $b = 2.1173 \times 10^{-11}\,\mathrm{m}^2$. Applying equation (3.28) gives

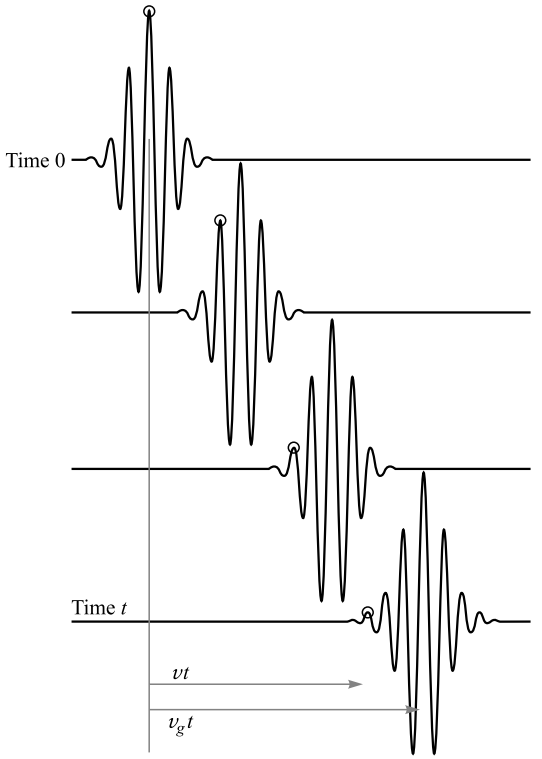

Figure 3.3. Dispersion of a modulated wave. The figure shows a sinusoidal wave that has been modulated by a Gaussian envelope, at four successive instants of time. After time t, a particular wave crest (shown by the circle) has moved a distance vt, whereas the peak of the modulating function has moved a distance $v_g t$. In this case, v is the phase velocity and v_g is the group velocity.

$$\frac{v_g}{c} = 1 - \frac{\lambda_0^2(a\lambda_0^2 + b)}{a(a+1)\lambda_0^4 + (1-2a)\lambda_0^2 + b^2}$$

Figure 3.4 shows the phase velocity v and the group velocity v_g, calculated from these formulae, for free-space wavelengths between 0.4 and 0.7 μm.

Returning to equation (3.24), which describes the dielectric constant of a metal (at sufficiently high frequencies) or a plasma, we note that above the plasma frequency the dielectric constant is real and less than 1. This means that the phase velocity v is greater than c, the speed of light, and at first sight this seems to contradict Einstein's principle that nothing can travel faster than c. However, as we remarked earlier, *information* is carried at the group velocity, not the phase velocity. It is easy to show, using equation (3.27), that if the dielectric constant is given by equation (3.24), then the relationship between v and v_g is

$$vv_g = c^2 \tag{3.29}$$

and so the group velocity is indeed less than c.

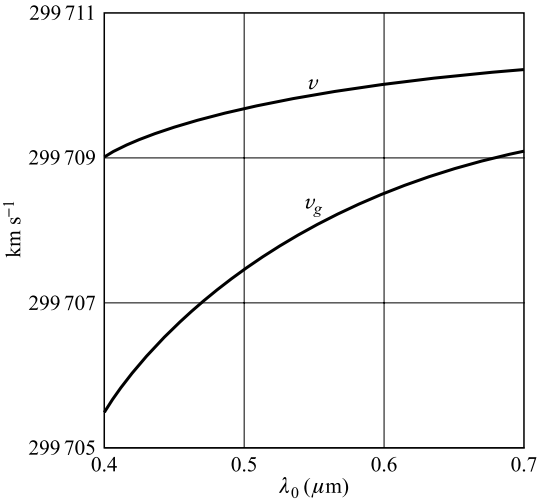

Figure 3.4. Phase and group velocities for light propagating in dry air at standard atmospheric pressure and 15°C.

3.2 Plane boundaries

In this section, we will review the phenomena of reflection and transmission when electromagnetic radiation encounters a plane boundary between two uniform homogeneous media (figure 3.5). We will call these media 1 and 2. The radiation is travelling in medium 1 towards the boundary with medium 2, and makes an angle θ_1 with the normal to the boundary. In general, some of the radiation will be reflected back into medium 1, again at an angle θ_1 but on the opposite side of the normal, and some will be refracted across the boundary so that it makes an angle θ_2 in medium 2. *Snell's law* relates the angles θ_1 and θ_2 through

$$n_1 \sin\theta_1 = n_2 \sin\theta_2 \tag{3.30}$$

where n_1 and n_2 are the refractive indices of the two media, and it also states that the incident, reflected and refracted rays, and the normal to the boundary, all lie in the same plane.

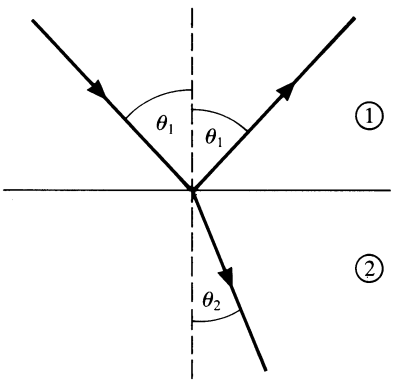

Figure 3.5. Reflection and refraction at a plane boundary between two media.

We will also need to know the reflection and transmission coefficients r and t. The reflection coefficient is defined as the electric field amplitude of the reflected radiation, expressed as a fraction of the electric field amplitude of the incident radiation, and similarly for the transmission coefficient. Since the values of these coefficients depend on the polarisation of the incident radiation, we will need to specify each coefficient for two orthogonal polarisations, giving a total of four coefficients. (The coefficients for any other polarisation state can be calculated by resolving the state into the components for the two states we have chosen, as shown in section 2.2.) The two polarisations that are usually chosen are called parallel and perpendicular, denoted by the symbols $\parallel$ and $\perp$ (figure 3.6). The term 'parallel polarisation' means that the electric field vector of the radiation is parallel to the plane containing the incident, reflected and refracted rays (and the normal to the boundary), and 'perpendicular polarisation' means that the electric field vector is perpendicular to this plane. Sometimes, especially in describing microwave systems, the terms 'horizontal polarisation' and 'vertical polarisation' are used instead. To understand this notation, it is necessary to think of the boundary as being horizontal, and to realise that 'vertically' polarised radiation merely has a vertical component. Provided that the two media are homogeneous, parallel-polarised incident radiation will give rise to parallel-polarised reflected and refracted radiation, and no perpendicularly polarised radiation. The converse of this statement is also true, so that perpendicularly polarised incident radiation does not produce any parallel-polarised components.

Now that we have defined our terms, we can proceed to state the formulae for the reflection and transmission coefficients. These are calculated, in terms of the impedances Z_1 and Z_2 of the media, by solving Maxwell's equations at the boundary:

$$r_\perp = \frac{Z_2 \cos\theta_1 - Z_1 \cos\theta_2}{Z_2 \cos\theta_1 + Z_1 \cos\theta_2} \tag{3.31.1}$$

$$t_\perp = \frac{2Z_2 \cos\theta_1}{Z_2 \cos\theta_1 + Z_1 \cos\theta_2} \tag{3.31.2}$$

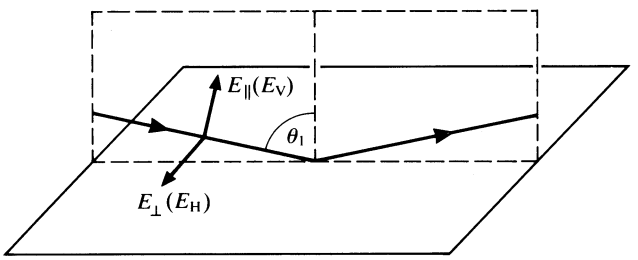

Figure 3.6. Parallel and perpendicular (vertical and horizontal) polarisations of radiation incident at and reflected from a plane boundary between two media.

$$r_{\parallel} = \frac{Z_2 \cos\theta_2 - Z_1 \cos\theta_1}{Z_2 \cos\theta_2 + Z_1 \cos\theta_1} \tag{3.31.3}$$

$$t_{\parallel} = \frac{2Z_2 \cos\theta_1}{Z_2 \cos\theta_2 + Z_1 \cos\theta_1} \tag{3.31.4}$$

The full expressions of equations (3.31) become rather complicated in the case where both media have significant absorption coefficients (i.e. the complex form of their refractive indices has to be taken into account). However, in many cases of practical importance we may assume that medium 1 has a refractive index of 1 (a vacuum, or air, to a good approximation). If medium 2 is absorbing, the Fresnel reflection coefficients for non-magnetic media are given by the following formulae:

$$r_{\perp} = \frac{\cos\theta_1 - \sqrt{\varepsilon_{r2} - \sin^2\theta_1}}{\cos\theta_1 + \sqrt{\varepsilon_{r2} - \sin^2\theta_1}} \tag{3.32.1}$$

$$t_{\perp} = \frac{2\cos\theta_1}{\cos\theta_1 + \sqrt{\varepsilon_{r2} - \sin^2\theta_1}} \tag{3.32.2}$$

$$r_{\parallel} = \frac{\sqrt{\varepsilon_{r2} - \sin^2\theta_1} - \varepsilon_{r2}\cos\theta_1}{\sqrt{\varepsilon_{r2} - \sin^2\theta_1} + \varepsilon_{r2}\cos\theta_1} \tag{3.32.3}$$

$$t_{\parallel} = \frac{2\sqrt{\varepsilon_{r2}}\cos\theta_1}{\sqrt{\varepsilon_{r2} - \sin^2\theta_1} + \varepsilon_{r2}\cos\theta_1} \tag{3.32.4}$$

Note that these expressions must in general be evaluated using complex arithmetic. If medium 1 has $n = 1$ and medium 2 is non-absorbing, the reflection coefficients become

$$r_{\perp} = \frac{\cos\theta_1 - \sqrt{n_2^2 - \sin^2\theta_1}}{\cos\theta_1 + \sqrt{n_2^2 - \sin^2\theta_1}} \tag{3.33.1}$$

$$r_{\parallel} = \frac{\sqrt{n_2^2 - \sin^2\theta_1} - n_2^2\cos\theta_1}{\sqrt{n_2^2 - \sin^2\theta_1} + n_2^2\cos\theta_1} \tag{3.33.2}$$

We can see from equation (3.33.2) that $r_{\parallel} = 0$ when θ_1 takes the value θ_B, given by

$$\tan\theta_B = n_2 \tag{3.34}$$

This is called the *Brewster angle*. Parallel (vertically) polarised radiation incident on a surface at the Brewster angle cannot be reflected, and so must all be transmitted into the medium. Consequently, we can note that randomly

polarised radiation incident from an arbitrary direction on a boundary between two media will in general, on reflection, be partially polarised, and if it is incident at the Brewster angle it will be completely plane-polarised. This is the simplest justification for the remark made in section 2.2 that the degree of polarisation is changed on reflection.

To illustrate equations (3.33) and the phenomenon of the Brewster angle, we will calculate the power reflection coefficients for light meeting an air–water interface. The refractive index of air can be taken as 1 and that of pure water as 1.333 with no imaginary part. Figure 3.7 shows the reflection coefficients as a function of the incidence angle θ_1. The figure shows that the value of $r_{\parallel}$ falls to zero near 50°, which is confirmed by calculating the Brewster angle from equation (3.34) as 53.1°. The figure also shows that when $\theta = 0$ the two reflection coefficients have the same value, which they must since for normally incident radiation there can be no distinction between parallel and perpendicular polarisations, and that when $\theta = 90°$ (grazing incidence) the power reflection coefficients are both 1 (i.e. all the radiation is reflected).

3.3 Scattering from rough surfaces

Scattering (reflection) of radiation from the Earth's surface is a fundamental process in most remote sensing situations. The exceptions to this principle are atmospheric sounding observations, and those passive observations (of thermal infrared or microwave emission) that do not respond to reflected sunlight. Thus, a consideration of the reflectance properties of real surfaces will be of considerable importance. In fact, as we saw in chapter 2, the thermal emissivity of a surface is directly related to its reflectance, so these properties will be important even in the case of passive microwave and thermal infrared remote sensing.

In section 3.2 we reviewed the behaviour of electromagnetic radiation when it is incident on a planar (i.e. perfectly smooth) boundary between two homogeneous media. In this section, we will consider radiation incident, from within

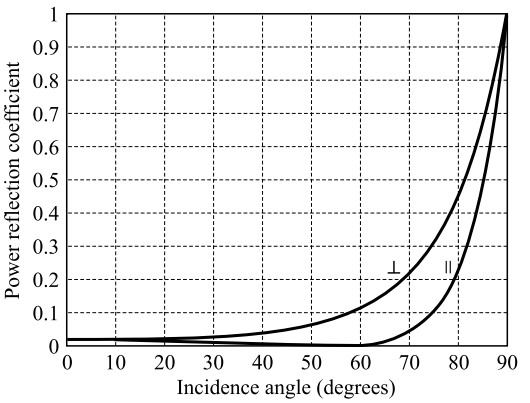

Figure 3.7. Power reflection coefficients for light incident on a water surface.

a vacuum (to which air is a reasonably good approximation), on a rough surface. The material below this surface will be assumed to be homogeneous, but we will consider what happens when it is *not* homogeneous in section 3.4.

3.3.1 Description of surface scattering

The first thing we need to do is to develop some of the terminology needed to describe rough-surface scattering. The treatment presented in this section is amplified in a number of works. Swain and Davis (1978) is a particularly useful source of information on quantitative descriptions of surface scattering in remote sensing, and Schanda (1986) also provides a helpful treatment. A more recent, and very full, discussion is provided by Hapke (1993).

Figure 3.8 shows a well-collimated beam of radiation of flux density F, measured in a plane perpendicular to the direction of propagation, incident on a surface at an angle θ_0. This angle is often called the *incidence angle*, and its complement $\pi/2 - \theta_0$ is the *depression angle*.[1] A proportion of the incident radiation will be scattered into the solid angle $d\Omega_1$, in a direction specified by the angle θ_1. For simplicity, the azimuthal angles have been omitted from figure 3.8. These will be denoted by ϕ_0 and ϕ_1, respectively.

The irradiance E at the surface is given by $F \cos \theta_0$. If we write $L_1(\theta_1, \phi_1)$, for the radiance of the scattered radiation in the direction (θ_1, ϕ_1), we can define the *bidirectional reflectance distribution function* (BRDF) R as

$$R = \frac{L_1}{E} \tag{3.35}$$

R has no dimensions, and its unit is sr^{-1}. It is also commonly represented by the symbols f or ρ. In considering radar systems (chapter 9), the BRDF is

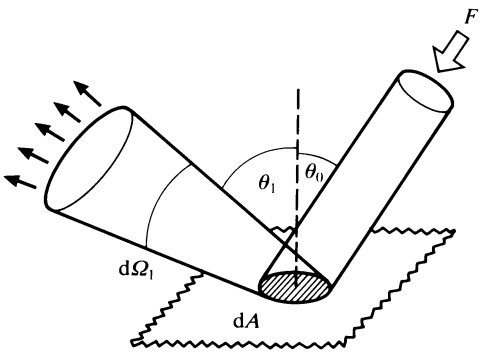

Figure 3.8. Radiation, initially of flux density F, is incident at angle θ_0 on an area dA and is then scattered into solid angle $d\Omega_1$ in the direction θ_1. The azimuthal angles ϕ_0 and ϕ_1 are omitted for clarity.

[1] This use of the term 'depression angle' assumes that the surface is horizontal. If not, it is probably safer to refer to the 'local incidence angle' and to avoid the term 'depression angle'.

usually replaced by the equivalent *bistatic scattering coefficient* γ, which has no units and is related to R by

$$\gamma = 4\pi R \cos\ \theta_1 \tag{3.36}$$

In fact, most radar systems, and all those we shall consider in chapter 9, detect only the *backscattered* component of the radiation, which retraces the path of the incident radiation. In this case, $\theta_1 = \theta_0$ and $\phi_1 = \phi_0$, and the usual way of specifying the proportion of scattered radiation is through the (dimensionless) *backscattering coefficient* σ^0, defined by

$$\sigma^0 = \gamma \cos\ \theta_0 = 4\pi R \cos^2\ \theta_0 \tag{3.37}$$

The BRDF is a function of the incidence and scattered directions (σ^0 is a function of the incidence direction only, since the scattered direction is the same), so in principle it should be written as a function of its arguments: $R(\theta_0, \phi_0, \theta_1, \phi_1)$. This notation is useful since it allows us to state the reciprocity relation obeyed by the BRDF:

$$R(\theta_0, \phi_0, \theta_1, \phi_1) = R(\theta_1, \phi_1, \theta_0, \phi_0) \tag{3.38}$$

but for compactness we will just write R, and take the arguments to be implied. In the majority of cases, the surface will lack azimuthally dependent features so that the dependence on ϕ_0 and ϕ_1 will simplify to a dependence on $(\phi_0 - \phi_1)$, and often the azimuthal dependence can be neglected altogether.

The *reflectivity* r of the surface is a function only of the incidence direction. It defines the ratio of the total power scattered to the total incident power. It is thus given by

$$r(\theta_0, \phi_0) = \frac{M}{E}$$

where M is the radiant exitance of the surface, and on substituting for M from equation (2.24) we find that

$$r(\theta_0, \phi_0) = \int_{\theta_1=0}^{\pi/2} \int_{\phi_1=0}^{2\pi} R \cos\ \theta_1 \sin\ \theta_1\ d\theta_1\ d\phi_1 \tag{3.39}$$

The reflectivity is also commonly called the *albedo* (from the Latin for 'whiteness') of the surface, and it is related to the emissivity ε in the direction (θ_0, ϕ_0) through

$$r = 1 - \varepsilon \tag{3.40}$$

We can define the *diffuse albedo* r_d, also called the *hemispherical albedo*, as the average value of r over the hemisphere of possible incidence directions. In this case, it represents the ratio of the total scattered power to the total incident power when the latter is distributed isotropically. Since the incident radiance is therefore constant, we may write it as L_0, so that the contribution dE to the irradiance from the direction (θ_0, ϕ_0) is $L_0 \cos\ \theta_0 \sin\ \theta_0\ d\theta_0\ d\phi_0$. The contribution dM that this makes to the radiant exitance in the direction (θ_1, ϕ_1) must

therefore be given by $RL_0 \cos\theta_0 \sin\theta_0\, d\theta_0\, d\phi_0 \cos\theta_1 \sin\theta_1\, d\theta_1\, d\phi_1$. The radiant exitance is thus

$$M = L_0 \int_{\theta_0=0}^{\pi/2} \int_{\phi_0=0}^{2\pi} \int_{\theta_1=0}^{\pi/2} \int_{\phi_1=0}^{2\pi} R \cos\theta_0 \sin\theta_0 \cos\theta_1 \sin\theta_1\, d\theta_0\, d\phi_0\, d\theta_1\, d\phi_1$$

and the irradiance is

$$E = L_0 \int_{\theta_0=0}^{\pi/2} \int_{\phi_0=0}^{2\pi} \cos\theta_0 \sin\theta_0\, d\theta_0\, d\phi_0 = \pi L_0$$

Since the diffuse albedo is given by M/E in this case, we can write it (making use of equation (3.39) to simplify the formula a little) as

$$r_\mathrm{d} = \frac{1}{\pi} \int_{\theta_0=0}^{\pi/2} \int_{\phi_0=0}^{2\pi} r(\theta_0, \phi_0) \cos\theta_0 \sin\theta_0\, d\theta_0\, d\phi_0 \tag{3.41}$$

3.3.2 *Simple models of surface scattering*

In this section, we will discuss a few of the important models of the BRDF of real surfaces. Further information can be found in, for example, Hapke (1993).

If the scattering surface is sufficiently smooth, it will behave like a mirror. This is called *specular scattering* or specular reflection (Latin *speculum* = a mirror). Radiation incident from the direction (θ_0, ϕ_0) will be scattered only into the direction $\theta_1 = \theta_0, \phi_1 = \phi_0 - \pi$, as illustrated schematically in figure 3.9a. The BRDF must therefore be a delta-function, and we can write it as

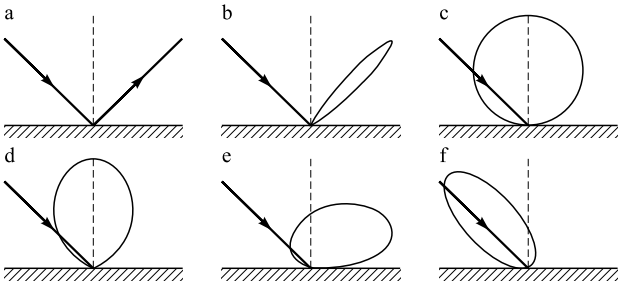

Figure 3.9. Schematic illustration of different types of surface scattering. The lobes are *polar diagrams* of the scattered radiation: the length of a line joining the point where the radiation is incident on the surface to the lobe is proportional to the radiance scattered in the direction of the line. (a) Specular reflection; (b) quasi-specular scattering; (c) Lambertian scattering; (d) Minnaert model ($\kappa = 2$); (e) Henyey–Greenstein model of forward scatter ($\Theta = 0.7$); (f) Henyey–Greenstein model of backscatter ($\Theta = -0.5$).

$$R = \frac{|r(\theta_0)|^2}{\cos\,\theta_0\,\sin\,\theta_0}\delta(\theta_1 - \theta_0)\;\delta(\phi_1 - \phi_0 + \pi) \tag{3.42}$$

where $r(\theta_0)$ is the appropriate Fresnel amplitude reflection coefficient for radiation with incidence angle θ_0. Inserting this expression into equation (3.39), we find that the reflectivity r for radiation with incidence angle θ_0 is just

$$r = |r(\theta_0)|^2$$

as of course it must be, and from equation (3.41) the diffuse albedo is

$$r_\mathrm{d} = 2\int_0^{\pi/2} |r(\theta_0)|^2 \cos\,\theta_0\,\sin\,\theta_0\,d\theta_0$$

Specular scattering is one limiting case of surface scattering, and it arises when the surface is very smooth (later we will consider just how smooth it needs to be). The other important limiting case is that of an ideally rough surface, giving *Lambertian scattering*. This has the property that, for any illumination that is uniform across the surface, the scattered radiation is distributed isotropically, and so the BRDF has a constant value. This is illustrated schematically in figure 3.9b. From equations (3.39) and (3.41) it can easily be seen that, for such a surface,

$$R(\theta_0, \phi_0, \theta_1, \phi_1) = r(\theta_0, \phi_0) = \frac{r_\mathrm{d}}{\pi} \tag{3.43}$$

Thus, for example, a Lambertian surface that scatters all of the radiation incident upon it has $R = 1/\pi$.

The scattering behaviour of real surfaces is often specified, not by using the BRDF, but instead by measuring the *bidirectional reflectance factor* (BRF). This is defined as the ratio of the flux scattered into a given direction by a surface under given conditions of illumination, to the flux that would be scattered in the same direction by a perfect Lambertian scatterer under the same conditions. The usefulness of this approach is that surfaces can be manufactured to have a BRF very close to unity for a fairly wide range of wavelengths and of incidence and scattering angles. The most common materials are barium sulphate, which, as a pressed powder and for $\theta < 45^\circ$, has a BRF greater than 0.99 for wavelengths between 0.37 and 1.15 μm, and magnesium oxide, which has a BRF greater than 0.98 over roughly the same range of conditions.

Although the Lambertian model is simple and idealised, the scattering from many natural surfaces can often, to a first approximation at least, be described using it. A simple modification is provided by the *Minnaert model*, in which the BRDF is given by

$$R \propto (\cos\,\theta_0\,\cos\,\theta_1)^{\kappa-1} \tag{3.44}$$

where the parameter κ has the effect of increasing or decreasing the radiance scattered in the direction of the surface normal (figure 3.9d). Lambertian scattering is the special case of the Minnaert model with $\kappa = 1$.

The scattering from real rough surfaces can often, as we have just remarked, be described by the Lambert or Minnaert models. However, neither of these models accounts for the fact that real surfaces may also show additional backscattering (where the radiation is scattered back into the incidence direction) or specular scattering. These can of course be incorporated by devising an empirical model that combines a Lambertian or Minnaert component with, for example, a 'quasi-specular' component. One common modification is to multiply the Lambert or Minnaert BRDF by the *Henyey–Greenstein* term

$$\frac{1-\Theta^2}{(1+2\Theta\cos g+\Theta^2)^{3/2}} \tag{3.45}$$

where the parameter Θ represents the anisotropy of the scattering, with $0 < \Theta \leq 1$ corresponding to forward scattering and $-1 \leq \Theta < 0$ corresponding to backscattering. The scattering phase angle g is given by

$$\cos g = \cos\theta_0 \cos\theta_1 + \sin\theta_0 \sin\theta_1 \cos(\phi_1 - \phi_0) \tag{3.46}$$

Figure 3.9e and f illustrate typical BRDFs that incorporate the Henyey–Greenstein term.

3.3.3 The Rayleigh roughness criterion

We have distinguished between the behaviour of a perfectly smooth surface and a Lambertian surface that is in some sense perfectly rough. It is clear that in order to understand which of these simple models is likely to give a better model of scattering from a real surface, some measure of surface roughness must be developed. The usual approach is via the Rayleigh criterion, which we will develop in this section.

Figure 3.10 shows schematically the detailed behaviour when radiation is incident on an irregular surface at angle θ_0, and scattered specularly from it at the same angle. We consider two rays: one is scattered from a reference plane,

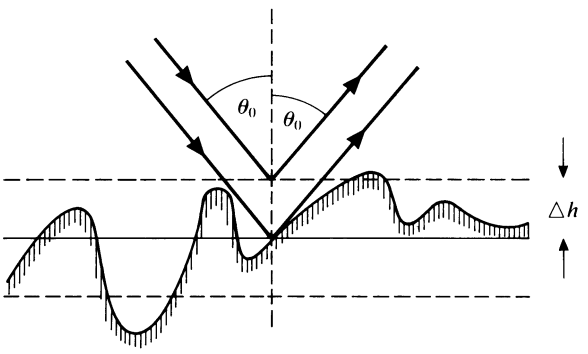

Figure 3.10. The Rayleigh criterion. Radiation is specularly reflected at an angle θ_0 from a surface whose r.m.s. height deviation is Δh. The difference in the lengths of the two rays is $2\Delta h \cos\theta_0$.

and the other from a plane at a height Δh above this reference plane. After scattering, the path difference between these two rays is $2\Delta h \cos\theta_0$, so the phase difference between them is

$$\Delta\phi = \frac{4\pi\,\Delta h\,\cos\,\theta_0}{\lambda}$$

where λ is the wavelength of the radiation. If we now let Δh stand for the root-mean-square (r.m.s.) variation in the surface height, $\Delta\phi$ becomes the root mean square variation in the phase of the scattered rays. A surface can be defined as smooth enough for scattering to be specular if $\Delta\phi$ is less than some arbitrarily defined value of the order of 1 radian. The conventional value is $\pi/2$, and this is called the Rayleigh criterion. Thus, for a surface to be smooth according to this criterion,

$$\Delta h < \frac{\lambda}{8\,\cos\,\theta_0} \tag{3.47}$$

Note that other criteria have also been adopted for the value of $\Delta\phi$ at which the surface becomes effectively smooth. A common definition that provides for the possibility of some intermediate cases between rough and smooth is that if $\Delta\phi$ is greater than $\pi/2$ the surface is rough, and if $\Delta\phi$ is less than $4\pi/25$ (so that the numerical part of the denominator in equation (3.47) becomes 25 instead of 8) it is smooth.

Equation (3.47) evidently dictates that for a surface to be effectively smooth at normal incidence, irregularities must be less than about $\lambda/8$ (or perhaps $\lambda/25$) in height. Thus, for a surface to give specular reflection at optical wavelengths (say $\lambda = 0.5\,\mu$m), Δh must be less than about 60 nm. This is a condition of smoothness likely to be met only in certain man-made surfaces such as sheets of glass or metal. On the other hand, if the surface is to be examined using VHF radio waves (say $\lambda = 3$ m), Δh need only be less than about 40 cm, a condition that could be met by a number of naturally occurring surfaces. A further aspect of equation (3.47) is the dependence on θ_0. The smoothness criterion is more easily satisfied at large values of θ_0 than at normal incidence, so that a moderately rough surface may be effectively smooth at glancing incidence. This fact is well known to anyone who has endured the glare of reflected sunlight from a low sun over an ordinary road surface. Although the scattering cannot really be described as specular in this case, the component of the BRDF in the specular direction is greatly enhanced.

3.3.4 Models for microwave backscatter

In this section, we shall discuss some of the commonest physical methods used to model the microwave backscatter from rough surfaces. This is a large and important area in which considerable research is still taking place, and the reader who wishes to pursue it in greater depth is recommended to study, for example, the books by Beckmann and Spizzichino (1963), Colwell (1983), Tsang et al. (1985) and Ulaby et al. (1981, 1986), and the more recent research

literature. The mathematical development of these models is generally rather difficult, and in this section we can do little more than sketch their principles.

3.3.4.1 *The small perturbation model*

The most helpful way to begin to look at the problem of microwave scattering from a rough surface is through the small perturbation model. This is essentially a Fraunhofer diffraction approach to rough-surface scattering, in which the interaction of the incident radiation with the surface is used to calculate the outgoing radiation field in the vicinity of the surface. This field can then be regarded as having been produced from a uniform incident radiation field by a fictitious screen that changes both the amplitude and the phase, and the far-field radiation pattern is obtained by calculating the Fraunhofer diffraction pattern of this screen.

In order to see how this is applied, but without becoming too deeply immersed in mathematical detail, we will consider a surface $z(x, y)$ in which the height z depends only on x, and which scatters all radiation incident upon it (i.e. the diffuse albedo is 1). Figure 3.11 illustrates radiation incident on the surface at angle θ_0 and scattered from it at angle θ_1. The rays AO and OB, of length a and b respectively, provide a reference from which phase differences can be measured. P is a point on the surface, that has coordinates x, $z(x)$. Simple trigonometry shows that the length of the ray CP is

$$a + x \sin \theta_0 - z(x) \cos \theta_0$$

and the length of the ray PD is

$$b - x \sin \theta_1 - z(x) \cos \theta_1$$

so the phase of the wave at D relative to the reference ray can be written as

$$\phi(x) = k\alpha x - k\beta z(x)$$

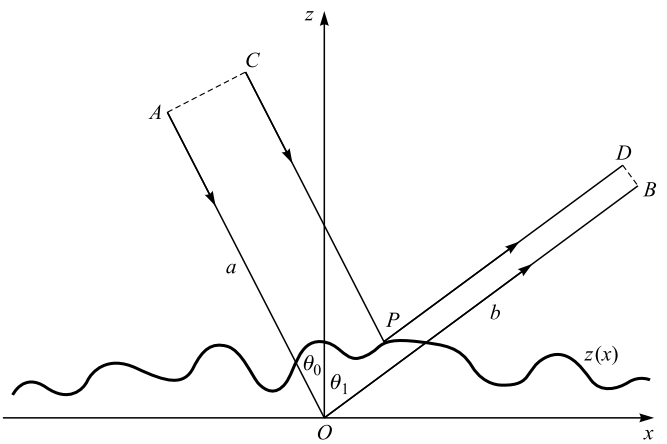

Figure 3.11. Model for developing the small perturbation model of rough-surface scattering.

where $\alpha = (\sin\theta_0 - \sin\theta_1)$, $\beta = (\cos\theta_0 + \cos\theta_1)$, and k is the wavenumber of the radiation. The total amplitude E scattered from the direction θ_0 into the direction θ_1 can therefore be written as

$$E = \int_{-\infty}^{\infty} e^{-i\phi(x)}\, dx = \int_{-\infty}^{\infty} e^{-ik\alpha x}\, e^{ik\beta z(x)}\, dx$$

This expression is clearly the Fourier transform of the function

$$e^{ik\beta z(x)}$$

which we can expand as a power series:

$$e^{ik\beta z(x)} = 1 + ik\beta z(x) - \frac{(k\beta z(x))^2}{2}\cdots \tag{3.48}$$

so that our expression for the scattered field amplitude becomes

$$E = \int_{-\infty}^{\infty} \left[1 + ik\beta z(x) - \frac{(k\beta z(x))^2}{2}\cdots\right] e^{-ik\alpha x}\, dx \tag{3.49}$$

The first term in this expression is a delta-function at $\alpha = 0$. Using the fact that $\alpha = (\sin\theta_0 - \sin\theta_1)$, we can see that this is just the specularly scattered component $\theta_1 = \theta_0$. We can write the second term as

$$ik\beta \int_{-\infty}^{\infty} z(x)\, e^{-ik\alpha x}\, dx$$

which is proportional to the Fourier transform of the surface height function $z(x)$. This suggests that it will be helpful to write the height function in terms of its Fourier transform $a(q)$, where q is the spatial frequency:

$$z(x) = \int_{-\infty}^{\infty} a(q)\, e^{iqx}\, dq$$

Thus, the second term in equation (3.49) becomes

$$ik\beta \int_{-\infty}^{\infty} \int_{-\infty}^{\infty} a(q)\, e^{i(q-k\alpha)x}\, dq\, dx$$

Using the definition of the Dirac delta-function that we met in section 2.3, we see that this can be written as

$$2\pi ik\beta \int_{-\infty}^{\infty} a(q)\delta(q - k\alpha)\, dq \tag{3.50}$$

This is the result that we need. It shows that the amplitude of the radiation scattered into the direction specified by α is proportional to the component of the surface height function with spatial frequency $q = k\alpha$.

There is another way of thinking about this result. The wave vector of the incident radiation has a horizontal component $k \sin \theta_0$ and the wave vector of the scattered radiation has a horizontal component $k \sin \theta_1$, so the term $k\alpha$ is just the change in this horizontal component. We can therefore say that the component of the scattered radiation amplitude is proportional to the spatial frequency component of the surface profile for which the spatial frequency corresponds to the change in the horizontal component of the radiation's wave vector.

Up to this point, we have assumed that the third and subsequent terms in the power-series expansion of equation (3.48) are negligible in comparison with the first two. If this is true, the phenomenon is known as *Bragg scattering*. Clearly, the condition that needs to be satisfied is

$$k\beta\,\Delta h \ll 1$$

which is equivalent to

$$\Delta h \ll \frac{\lambda}{2\pi(\cos\ \theta_0 + \cos\ \theta_1)}$$

Thus, the surface must be smooth according to the Rayleigh roughness criterion (3.47). The Bragg scattering mechanism is thought to be largely responsible for the reflection of microwave radiation from small-scale (of the order of 1 cm) roughness on water surfaces, especially where the structure of this roughness contains a dominant spatial frequency, in which case the Bragg scattering is said to be *resonant*.

We have also assumed that the surface height z depends only on the x-coordinate. A more general derivation for two-dimensional isotropic surfaces, which more or less follows the argument we have just presented, leads to the following expression for the backscattering coefficient σ^0:

$$\sigma^0_{pp} = 4k^4L^2(\Delta h)^2 \cos^4\ \theta |f_{pp}(\theta)|^2 \exp(-k^2L^2\ \sin^2\ \theta) \tag{3.51}$$

In this expression, σ^0_{pp} is the backscattering coefficient for pp-polarisation (so that, for example, $p = \mathrm{H}$ means HH-polarisation, or radiation both incident and scattered in the horizontal polarisation state), θ is the incidence angle of the radiation, L is the correlation length[2] of the surface (i.e. the 'width' of the irregularities, which contains information about the shape of the spatial frequency spectrum of the surface), and $f_{pp}(\theta)$ is a measure of the surface reflectivity for radiation with incidence angle θ. For HH-polarised radiation we have

[2] In fact, equation (3.51) is based on the assumption that the surface has a Gaussian autocorrelation function. L is the distance over which the autocorrelation coefficient falls to a value of $1/e$. See box for more information.

$$f_{\mathrm{HH}}(\theta) = \frac{\cos\theta - \sqrt{\varepsilon_r - \sin^2\theta}}{\cos\theta + \sqrt{\varepsilon_r - \sin^2\theta}} \tag{3.52.1}$$

which is just the Fresnel reflection coefficient for radiation incident at angle θ from a vacuum onto the surface of a medium with a (complex) dielectric constant ε_r. For VV-polarised radiation, the corresponding formula is

$$f_{\mathrm{VV}}(\theta) = (\varepsilon_r - 1)\frac{\sin^2\theta - \varepsilon_r(1 + \sin^2\theta)}{\left(\varepsilon_r \cos\theta + \sqrt{\varepsilon_r - \sin^2\theta}\right)^2} \tag{3.52.2}$$

The conditions for the validity of equation (3.51) are usually given as

$$k\Delta h < 0.3 \tag{3.53.1}$$

and

$$kL < 3 \tag{3.53.2}$$

although these are somewhat approximate.

Figure 3.12 illustrates the backscatter predicted by the small perturbation model for a surface with $\varepsilon_r = 10$. In each case, the r.m.s. height variation Δh is the same. It can be seen that the effect of increasing kL, the spatial scale of the surface roughness features, is to increase the specular scattering ($\theta = 0$) at the

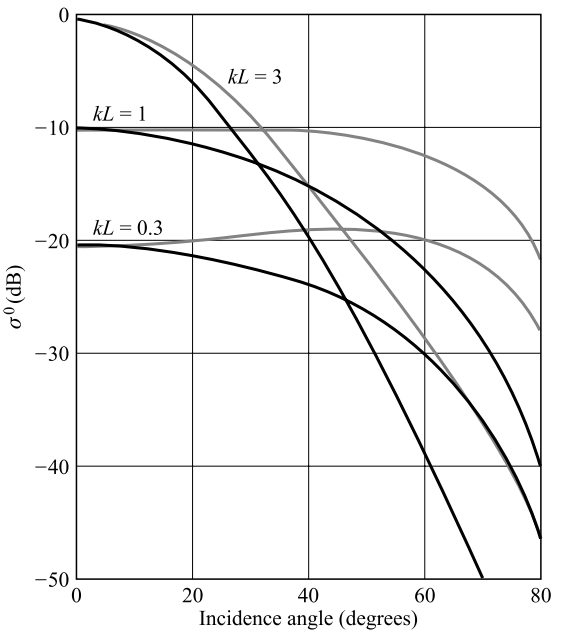

Figure 3.12. Backscatter calculated according to the small perturbation model for a surface having dielectric constant $\varepsilon_r = 10$. In each case, $k\,\Delta h = 0.3$ and the curves are labelled with the values of kL. The black curves are for HH-polarisation and the grey curves are for VV-polarisation.

THE AUTOCORRELATION FUNCTION

The r.m.s. height variation Δh is the simplest measure of the roughness of a surface, but it tells us nothing about the *scale* of the irregularities. The autocorrelation function provides this information.

Suppose (for simplicity) we consider a one-dimensional surface $z(x)$, where z is the height at position x. The mean height is $\langle z \rangle$, where the angle brackets denote an average over all values of x, and the r.m.s. height variation is defined by

$$\Delta h = \left\langle (z(x) - \langle z \rangle)^2 \right\rangle^{1/2}$$

The autocorrelation function is defined by

$$\rho(\xi) = \frac{\left\langle (z(x+\xi) - \langle z \rangle)(z(x) - \langle z \rangle) \right\rangle}{\Delta h^2}$$

and is measure of the similarity of the heights at two points separated by distance ξ. By the definition, $\rho(0) = 1$, and for most surfaces, $\rho(\infty) = 0$. Common models for the autocorrelation function are the Gaussian

$$\rho(\xi) = \exp\left(-\frac{\xi^2}{L^2}\right)$$

and the negative exponential

$$\rho(\xi) = \exp\left(-\frac{\xi}{L}\right)$$

In each case, L (the correlation length) is a measure of the width of the irregularities of the surface.

The extension of this idea to two dimensions is straightforward.

expense of the scattering at larger angles. Since the root-mean-square surface slope is of the order of $\Delta h/L$, increasing the value of kL while keeping the value of $k\,\Delta h$ constant corresponds to decreasing the r.m.s. surface slope, so it is not surprising that this increases the specular component of the scattering. The effect of varying $k\,\Delta h$, not shown in the figure, is very straightforward since equation (3.51) shows that the backscatter coefficient is just proportional to $(\Delta h)^2$. Thus, decreasing $k\,\Delta h$ by a factor of 10, say, would have the effect of shifting all the curves in the figure down by 20 dB without changing their shapes.

3.3.4.2 *The Kirchhoff model*

The approach that is adopted by the Kirchhoff model for scattering from randomly rough surfaces is to model the surface as a collection of variously oriented planes, each of which is locally tangent to the surface. This is called the *tangent plane approximation*. The scattered radiation field can then be calculated using the results for radiation incident on a plane interface. Two variants of the Kirchhoff model are in common use: the *stationary phase* (or *geometric optics*) *model*, which is valid for rougher surfaces, and the *scalar approximation*.

The backscatter coefficient is given by the stationary phase model as

$$\sigma^0_{HH}(\theta) = \sigma^0_{VV}(\theta) = \frac{|r(0)|^2 \exp\left(-\dfrac{\tan^2\,\theta}{2m^2}\right)}{2m^2\,\cos^4\,\theta} \tag{3.54}$$

where $r(0)$ is the Fresnel reflection coefficient for normally incident radiation, and m is the root-mean-square surface slope. For a surface having a Gaussian autocorrelation function with correlation length L and root-mean-square height variation Δh,

$$m = \sqrt{2}\frac{\Delta h}{L} \tag{3.55}$$

The conditions for the validity of this model are

$$k\,\Delta h\,\cos\,\theta > 1.58 \tag{3.56.1}$$

$$kL > 6 \tag{3.56.2}$$

and

$$kL^2 > 17.3\;\Delta h \tag{3.56.3}$$

The backscatter coefficient is given by the scalar approximation as

$$\sigma^0_{pp}(\theta) = k^2L^2\cos^2\theta|r_p(\theta)|^2\exp(-4k^2\Delta h^2\cos^2\theta)$$

$$\times\sum_{n=1}^{\infty}\frac{(2k\,\Delta h\,\cos\,\theta)^{2n}}{n!n}\exp\left(-\frac{k^2L^2\,\sin^2\,\theta}{n}\right) \tag{3.57}$$

where we have again assumed that the autocorrelation function of the surface is Gaussian. $r_p(\theta)$ is the Fresnel coefficient for p-polarised radiation incident at angle θ. The conditions for the validity of this model are

$$\Delta h < 0.18L \tag{3.58.1}$$

$$kL > 6 \tag{3.58.2}$$

and

$$kL^2 > 17.3\;\Delta h \tag{3.58.3}$$

We can note that the second and third of these conditions are the same as for the stationary phase model.

Figure 3.13 illustrates the backscatter predicted by both variants of the Kirchhoff model for a surface with $\varepsilon_r = 10$. In each case, the value of kL has been kept constant. Two sets of curves show the predicted backscatter from a smooth ($k\,\Delta h = 3$) and rough ($k\,\Delta h = 10$) surface. Again, we see that smoother surfaces give enhanced scattering near the specular direction.

There are, in fact, further restrictions on the validity of the Kirchhoff model that we should note. As was mentioned above, the first step in constructing the model is to replace the surface by a set of planes or facets, each of which is locally tangent to the surface. It is clear that, for this programme to succeed, we must be able to define facets whose spatial extent is much greater than the wavelength λ (so that diffraction effects do not dominate), but whose deviation from the real surface is much less than λ (so that we do not incur large phase errors in modelling the surface). This is, in fact, a restriction on the local curvature of the surface, as we can see by the following simple one-dimensional argument.

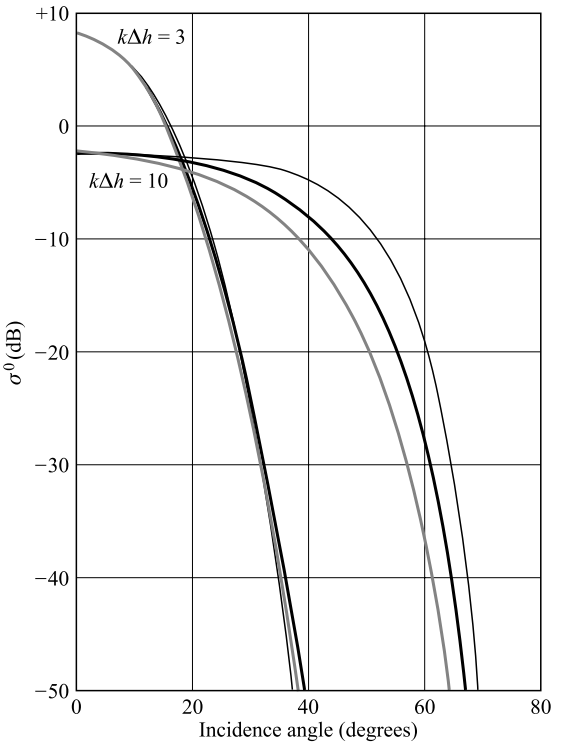

Figure 3.13. Backscatter calculated according to the Kirchhoff model for a surface having dielectric constant $\varepsilon_r = 10$. In each case, $kL = 30$, and the curves are labelled with the values of $k\,\Delta h$. The thin black curves are for the stationary phase model, the thick black curves are for the scalar approximation for HH-polarisation, and the thick grey curves are for the scalar approximation for VV-polarisation.

We will assume that, locally, the surface has a constant radius of curvature R, so that it forms part of a sphere or, in one dimension, a circle. Figure 3.14 shows a facet of length $2w$ tangent to this circle. The facet subtends an angle 2ψ at the centre of curvature, where $\psi = \tan^{-1}(w/R)$, and the maximum deviation of the facet, x, from the surface is $R(\sec\psi - 1)$. If $w \ll R$, this can be approximated as $x \approx w^2/2R$. Now we will assume that $w > \lambda$ (so that the facet is large enough for diffraction effects not to dominate) and that $x < \lambda/2$ (so that we do not incur large phase errors in approximating the surface by the facet). Thus, we obtain the condition that $R > \lambda$. In other words, in order for the surface to be adequately represented by facets, its radius of curvature must exceed a few wavelengths.

Another condition that must be satisfied is that the incidence or scattering angles should not be so large that one part of the surface can obscure another. If this occurs in practice, it can usually be dealt with by an appropriate modification of the model, or by specifying that the model is valid only up to some maximum angle.

3.3.4.3 Other models

It is clear that the models of backscatter from randomly rough surfaces that we have considered in the two preceding sections do not provide a complete description of the possible phenomena. Firstly, we can note that the ranges of validity of the three models that we have discussed, defined in equations (3.53), (3.56) and (3.58), do not cover all the possibilities. This fact is illustrated in figure 3.15, which shows the valid range of each model in terms of the dimensionless parameters $(\Delta h/\lambda)$ and (L/λ). Secondly, we can note from figure 3.13 that, even where two models are both apparently valid, they can give different predictions for the backscatter. This is to some extent a consequence of the approximations inherent in the models. Thirdly, we can observe that none of the three models that has been discussed has an explicit dependence on

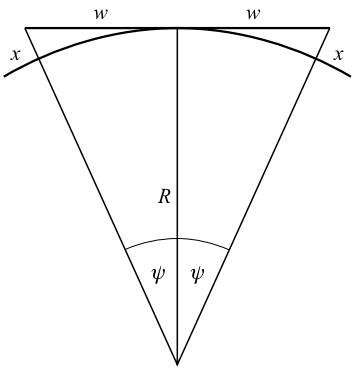

Figure 3.14. A one-dimensional facet of length $2w$ is tangent to a surface with radius of curvature R. The facet subtends an angle 2ψ at the centre of curvature, and its maximum deviation from the surface is x.

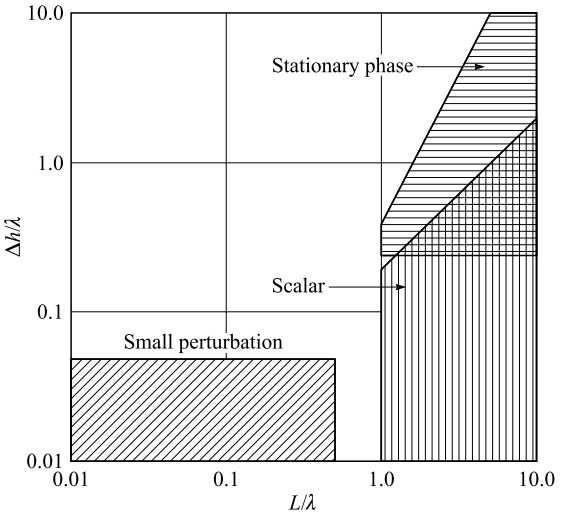

Figure 3.15. Range of validity of the small perturbation, stationary phase and scalar approximation models of rough-surface scattering. For the stationary phase model, the incidence angle has been taken as zero.

the imaginary part of the dielectric constant, which is in contradiction to the experimental evidence.

Many of these difficulties can be circumvented by the use of the *integral equation model*. This is still an approximation, but its grounding in the physics of the interactions between the radiation and the surface is more nearly fundamental. The integral equation model has a larger region of validity and is sensitive to both the real and the imaginary parts of the dielectric constant. It is thus useful for estimating these parameters from backscattering measurements. Unfortunately, its mathematical complexity is such that it is beyond our scope to discuss it any further here.

3.4 Volume scattering

In sections 3.2 and 3.3 we have considered the scattering of electromagnetic radiation from the boundary between two media, for example at the interface between a vacuum (to which air may be a good approximation) and some surface material. Unless the transmission coefficient of the interface is zero, some fraction of the radiation will also enter the material beyond the interface and hence have the possibility of interacting with the bulk of the material as well as with its surface. First, we discuss what happens if this material is homogeneous but absorbing. For simplicity, we will consider the situation shown in figure 3.16. Radiation is incident normally, from a vacuum, onto a parallel-sided slab of medium 1 of thickness d. Below this slab is an infinitely thick slab of medium 2.

The incident radiation has unit amplitude, so the ray A has amplitude r_{01}, defined as the amplitude reflection coefficient for radiation incident from med-

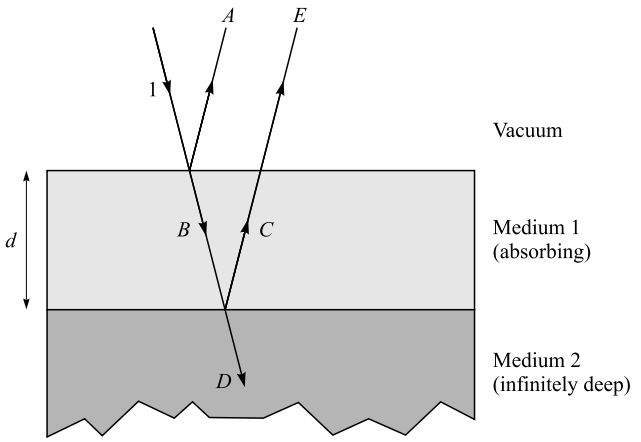

Figure 3.16. Radiation incident normally on a slab of medium 1 of thickness d, underlain by an infinitely thick slab of medium 2. The rays have been shown at an angle for clarity.

ium 0 (vacuum) onto medium 1. However, it is clear from figure 3.16 that there may be an additional contribution E to the radiation reflected from this system. The ray B has amplitude t_{01}, at the top of medium 1, so at the bottom of this slab it must have amplitude $t_{01}\mathrm{e}^{-ikd}$, where k is the (complex) wavenumber of the radiation in medium 1. A fraction r_{12} of this is reflected at the interface between media 1 and 2, so the amplitude of the ray C at the bottom of medium 1 is $t_{01}r_{12}e^{-ikd}$, and the amplitude of this ray at the top of the slab is therefore $t_{01}r_{12}e^{-2ikd}$. Finally, we can write the amplitude of the ray E as $t_{01}r_{12}t_{10}\mathrm{e}^{-2ikd}$.

Adding together the contributions from rays A and E, we see that the reflection coefficient has become

$$r_{01} + t_{01}r_{12}t_{10}e^{-2ikd}$$

We have ignored the ray D in this analysis. This is correct, because medium 2 is infinitely thick so there is no interface to reflect this radiation back into medium 1. We have also ignored the possibility that the ray C can be reflected back into medium 1, and in fact the radiation can bounce between the upper and lower surfaces of medium 1 indefinitely, with a little more radiation escaping upwards at each reflection from the upper surface. When this is taken into account, the formula for the reflection coefficient of the system becomes

$$r_{01} + \frac{t_{01}r_{12}t_{10}\,\exp(-2ikd)}{1 - r_{10}r_{12}\,\exp(-2ikd)} \tag{3.59}$$

Figure 3.17 illustrates the behaviour of this function (or rather, the power reflection coefficient which is the square of its magnitude) as a function of the slab thickness d, for the case where medium 1 has $\varepsilon_r = 10 - 2i$ and medium 2 has $\varepsilon_r = \infty$ (i.e. is perfectly reflecting). The frequency is 1 GHz. (These dielectric constants are not intended to correspond to any particular real materials, and are just for illustration.) The figure shows that, when medium 1 has a thickness of zero, the power reflection coefficient is equal to that of the inter-

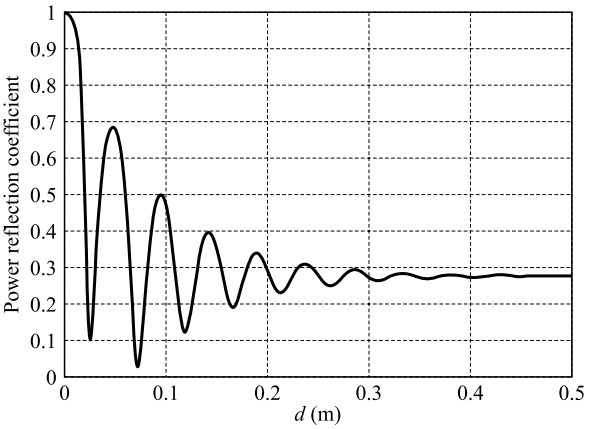

Figure 3.17. Power reflection coefficient at normal incidence and 1 GHz for a slab of material with $\varepsilon_r = 10 - 2i$ and thickness d overlying a perfectly reflecting surface.

face between media 1 and 2. When medium 2 is sufficiently thick, the power reflection coefficient is equal to that of the upper surface of medium 1. This is easy to understand from figure 3.16. If d is sufficiently large, the ray B is attenuated practically to zero as it travels down through medium 1, so there is nothing left to be reflected back as ray C. From equations (3.12) and (3.15) we can calculate the absorption length in medium 1 to be 0.076 m, so we can see from figure 3.17 that this situation is reached in practice once the depth of the layer is of the order of five absorption lengths. We also note from figure 3.17 that the reflection coefficient oscillates, with a diminishing amplitude, as d increases. These oscillations are due to interference between the emerging rays.

Although we have considered only a simple example, it is clear from the analysis we have just performed that, if there is *no* second medium underneath medium 1 (or, equivalently, if medium 1 is sufficiently thick), none of the radiation that enters medium 1 will be reflected back out of it. In this case, only surface scattering can occur. However, this assumes that the medium is homogeneous. If the medium is inhomogeneous – 'lumpy' – the inhomogeneities can *scatter* radiation. This phenomenon will be discussed in the next section.

3.4.1 The radiative transfer equation

To begin with, we will develop a model of the behaviour of radiation when both absorption and scattering are present. We have already encountered the phenomenon of absorption. In section 3.1.1 we defined the absorption length and noted (from equations (3.14) and (3.15)) that, for radiation propagating in the z-direction in a medium with absorption length l_a, the flux density [3] F varies according to

[3] Note that throughout this section we are considering only the *intensity* of radiation, not its *amplitude*, and we will not therefore have the added complcation of interference effects, such as those illustrated in figure 3.17. In effect, we are assuming that the scattering phenomena are *incoherent*.

$$F = F_0 \exp\left(-\frac{z}{l_a}\right)$$

where F_0 is a constant. This can also be written as a differential equation:

$$\frac{dF}{dz} = -\frac{F}{l_a}$$

in which case it is valid even if l_a varies with z, but it is more usual to write this expression as

$$\frac{dF}{dz} = -\gamma_a F \tag{3.60}$$

where $\gamma_a = 1/l_a$ is the *absorption coefficient*. A helpful way to visualise the meaning of this equation is to consider radiation of flux density F incident normally on a thin slab of absorbing material of thickness Δz. Rearranging equation (3.60) very slightly, we see that $(\Delta F)/F = -\gamma_a \Delta z$, so that the *fraction* of the incident power that is absorbed by the slab is $\gamma_a \Delta z$. The fraction absorbed is proportional to the thickness, as we would expect (as long as the slab is thin), and γ_a is just the coefficient of proportionality.

Scattering can be defined as the deflection of electromagnetic radiation, without absorption, as a result of its interaction with particles (electrons, atoms, molecules or larger particles) or a solid or liquid surface. We will consider the nature of scattering by particles in the following sections, but for the present it will be enough to define the *scattering coefficient*. This is very similar to the definition of the absorption coefficient: a thin slab, of thickness Δz, scatters a fraction $\gamma_s \Delta z$ of the power incident upon it, where γ_s is the scattering coefficient. Of course, the scattered radiation is not 'lost', unlike the absorbed radiation, and we need to keep track of it.[4] In order to see how the radiative transfer equation works, we will first derive a simplified, one-dimensional version of it.

Figure 3.18 shows radiation propagating the $+z$ and $-z$ directions in three adjacent parallel slabs, each of thickness Δz. We have used the symbols F_+ and F_- to represent the flux densities propagating in the two directions. When radiation is incident on one of these slabs, a fraction $\gamma_a \Delta z$ is absorbed and a fraction $\gamma_s \Delta z$ is scattered. We assume that all of this scattered radiation is scattered backwards, so that the fraction of the radiation that is transmitted through the slab is $1 - (\gamma_a + \gamma_s)\Delta z$. It is clear from figure 3.18 that the the flux density F_+ in the middle slab is contributed to by the transmitted component of

[4] We are considering only *elastic* scattering, in which the wavelength of the radiation is unchanged by the scattering process. Thus, we are neglecting the phenomenon of *fluorescence*, in which radiation is absorbed at one wavelength and re-emitted at another, usually longer. Some minerals, especially sulphides, fluoresce in the visible part of the spectrum when excited by ultraviolet radiation. Plant material also shows a diagnostically useful fluorescence response. However, most fluorescence phenomena are too small to be measured accurately from airborne or (especially) spaceborne observations. Cracknell and Hayes (1991) give a useful discussion of 'fluorosensing'.

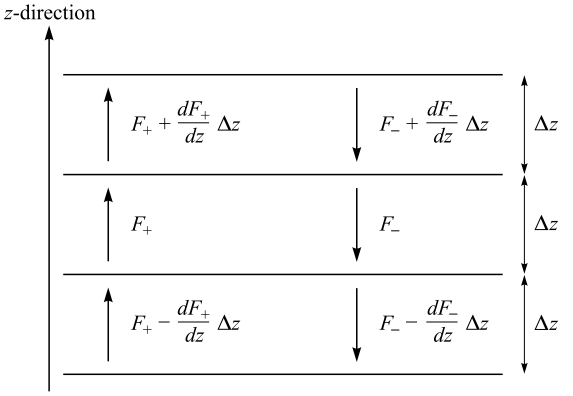

Figure 3.18. Radiation propagating in the $+z$ and $-z$ directions in three parallel slabs of thickness Δz.

the positive-direction flux in the lower slab, and the reflected (scattered) component of the negative-direction flux in the middle slab, so we must have

$$F_+ = \left(F_+ - \frac{dF_+}{dz}\Delta z\right)(1 - (\gamma_a + \gamma_s)\ \Delta z) + F_-\gamma_s\ \Delta z$$

Ignoring the terms in $(\Delta z)^2$ and rearranging, we find

$$\frac{dF_+}{dz} = -(\gamma_a + \gamma_s)F_+ + \gamma_s F_- \tag{3.61.1}$$

This is an intuitively reasonable equation. It shows that radiation is being lost from the forward direction as a result of both absorption and scattering, but gained from the scattering of backward-travelling radiation. The corresponding equation for the backward-travelling radiation is

$$\frac{dF_-}{dz} = (\gamma_a + \gamma_s)F_- - \gamma_s F_+ \tag{3.61.2}$$

We can note from these equations the significance of the *sum* of the absorption and scattering coefficients in describing the propagation of radiation where both phenomena are important, since it represents the loss of energy from the forward-propagating radiation. This combination of absorption and scattering is usually called *attenuation* (sometimes *extinction*), and the attenuation coefficient is defined as

$$\gamma_e = \gamma_a + \gamma_s \tag{3.62}$$

Equation (3.61) can be used to identify some of the important consequences of volume scattering. We will consider an infinitely deep slab of material in which the absorption and scattering coefficients are constant, and radiation of unit flux density incident normally on the slab. To keep things as simple as possible, we will also assume that the reflection coefficient at the surface of this slab is zero, so that only volume scattering is important. This situation is described by equations (3.61.1) and (3.61.2) in the region $z \leq 0$, and subject

to the boundary conditions that $F_-(0) = 1$, $F_+(-\infty) = F_-(-\infty) = 0$. It is not difficult to show that the solution is

$$F_- = \exp(\mu z)$$
$$F_+ = \frac{\gamma_a + \gamma_s - \mu}{\gamma_s} \exp(\mu z)$$

where

$$\mu = \sqrt{\gamma_a^2 + 2\gamma_a\gamma_s}$$

so the intensity reflection coefficient is

$$R = \frac{\gamma_a + \gamma_s - \sqrt{\gamma_a^2 + 2\gamma_a\gamma_s}}{\gamma_s} \tag{3.63}$$

This function, which depends only on the *ratio* of γ_s to γ_a, is shown in figure 3.19.

Figure 3.19 shows that, if the scattering coefficient is much larger than the absorption coefficient, the volume scattering will be large. This is the reason that many finely divided materials, such as snow, clouds and (for example) table salt, are white. The total optical absorption in a slab of pure ice 1 m thick is small, but if the ice is divided up into snow grains each of which is only 1 mm across, a ray of light will encounter 2000 ice–air interfaces as it traverses the snow layer. Scattering can occur at each of these interfaces, and although the amount of scattering at each interface is small, the cumulative effect is large. Provided the absorption coefficient is small across the whole of the visible spectrum, as it is for ice, water and sodium chloride, the material will therefore appear white.

Equations (3.61) can only strictly be applied to problems in which the scattering of radiation is all backwards, opposite to the direction of incidence. In general, scattered radiation will be distributed over all possible directions, and

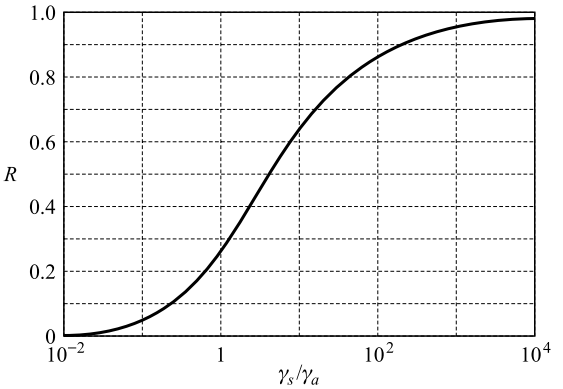

Figure 3.19. Dependence of the intensity reflection coefficient R for volume scattering on the ratio of the scattering coefficient to the absorption coefficient (one-dimensional model).

a simple one-dimensional approach to the problem is no longer possible. To describe this situation, we will need to use the *radiance* of the radiation, and to consider its distribution with direction as well as position. However, the essential principles remain the same. In three dimensions, if only absorption and scattering are involved, the radiative transfer equation becomes

$$\frac{dL_f(\theta, \phi)}{dz} = -(\gamma_a + \gamma_s)L_f(\theta, \phi) + \gamma_s J_f \tag{3.64}$$

where $L_f(\theta, \phi)$ is the spectral radiance propagating in the direction (θ, ϕ), and dz measures distance in this same direction. J_f describes the radiation scattered into the direction (θ, ϕ) from other directions specified by (θ', ϕ'), and is defined by

$$J_f = \frac{1}{4\pi} \int_{4\pi} L_f(\theta', \phi') p(\cos \Theta)\, d\Omega' \tag{3.65}$$

where $d\Omega' = \sin \theta'\, d\theta'\, d\phi'$ is an element of solid angle, and the integration is performed over all directions (i.e. over 4π steradians). $p(\cos \Theta)$ is the *phase function* of the scattering, and describes the angular distribution of the scattered radiation in terms of the angle Θ through which the radiation has been deflected. This angle is given by

$$\cos \Theta = \cos \theta \cos \theta' + \sin \theta \sin \theta' \cos(\phi - \phi') \tag{3.66}$$

Further modifications to equation (3.64) are possible. The only one we will consider now is the effect of black-body emission. If the radiation is in thermal equilibrium with the medium through which it is propagating, we need to add a term for emission to equation (3.64):

$$\frac{dL_f(\theta, \phi)}{dz} = -(\gamma_a + \gamma_s)L_f(\theta, \phi) + \gamma_s J_f + \gamma_a B_f \tag{3.67}$$

where B_f is the spectral radiance of black-body radiation at the appropriate temperature T, given by equation (2.30):

$$B_f = \frac{2hf^3}{c^2} \frac{1}{\exp(hf/kT) - 1} \tag{3.68}$$

Various special cases of equation (3.67) find important applications in different aspects of remote sensing. We will consider first the case in which only absorption is significant, so that we can set γ_s and B_f to zero. This gives the equation

$$\frac{dL_f}{dz} = -\gamma_a L_f$$

which is equivalent to equation (3.60). Note that we do not need to specify the direction (θ, ϕ), because there is no scattering so the direction does not change. If γ_a varies with position z, the solution of this equation can be written as

$$L_f(z) = L_f(0) \exp(-\tau(z)) \tag{3.69}$$

where

$$\tau(z) = \int_0^z \gamma_a(z')\, dz' \tag{3.70}$$

is the integral of the absorption coefficient with respect to distance from 0 to z. This quantity τ is called the *optical thickness* of the path from 0 to z.

Next, we will add thermal emission back into our model, but will continue to ignore scattering. The radiative transfer equation in this case is

$$\frac{dL_f}{dz} = \gamma_a(B_f - L_f) \tag{3.71}$$

If the frequency is low enough for the Rayleigh–Jeans approximation to be valid, this can be rewritten as

$$\frac{dT_b}{dz} = \gamma_a(T - T_b)$$

where T_b is the brightness temperature of the radiation and T is the physical temperature of the medium through which it is propagating. For constant T, the solution to this equation is

$$T_b(z) = T_b(0)\, \exp(-\tau(z)) + T(1 - \exp(-\tau(z))) \tag{3.72}$$

Equation (3.72), which has an obvious application to the correction of microwave radiometer measurements for the effect of atmospheric absorption, has an intuitive reasonableness. If radiation travels through only a small amount of absorbing material, so that τ is small, the brightness temperature is hardly changed; but if the optical thickness is large, the brightness temperature of the emerging radiation is equal to the physical temperature of the medium.

Finally, we will consider the solution of equation (3.71) in the case where B_f is not constant because the temperature is not constant. This could be, for example, a model of atmospheric temperature sounding, where the brightness temperature of upward-travelling radiation is measured at a point above the bulk of the Earth's atmosphere and used to make deductions about the temperature distribution within the atmosphere. It is much simpler in this case to work with the optical thickness τ rather than the position z, and we can note from equation (3.70) that there is a monotonic relationship between τ and z. On this basis, the solution of equation (3.71) can be written as

$$L_f(\tau) = L_f(0)\, \exp(-\tau) + \int_0^\tau B_f(\tau')\, \exp(\tau' - \tau)\, d\tau' \tag{3.73}$$

or, if the Rayleigh–Jeans approximation is valid, as

$$T_b(\tau) = T_b(0)\, \exp(-\tau) + \int_0^\tau T(\tau')\, \exp(\tau' - \tau)\, d\tau' \tag{3.74}$$

As before, an intuitive understanding of these equations is possible. For simplicity, we will consider equation (3.74), and assume that it applies to radiation propagating upwards from the Earth's surface (where z and τ are zero), through the atmosphere, for some total distance $z_{\max}$ (see figure 3.20). The brightness temperature of the radiation emitted from the Earth's surface is $T_b(0)$, and the total optical thickness of the path is τ, so the first term in equation (3.74) corresponds to equation (3.69) and just represents the absorption of the surface radiation. The integrand considers some position z such that the optical thickness between this point and $z = 0$ is τ'. The optical thickness between this point and $z = z_{\max}$ is $(\tau - \tau')$, so we expect the contribution from this point to be reduced by a factor of $\exp(-(\tau - \tau'))$. The optical thickness $(\tau - \tau')$ from the point in the atmosphere from which the radiation originates, to the point at which it is measured, is often called the *optical depth* of the former point.

3.4.2 Absorption and scattering by macroscopic particles

In section 3.4.1, we introduced the concepts of the absorption and scattering coefficients. These were defined as bulk properties of the medium through which the radiation is propagating, but they arise from interactions between the radiation and the particles of which the medium is composed. In this section, we will examine the factors that relate the absorption and scattering coefficients to physical properties of the particles.[5] We begin by assuming that the particles are much smaller than the wavelength of the radiation, so that the electric field at any instant can be assumed to be constant across the particle. However, we will defer a discussion of scattering and absorption by individual

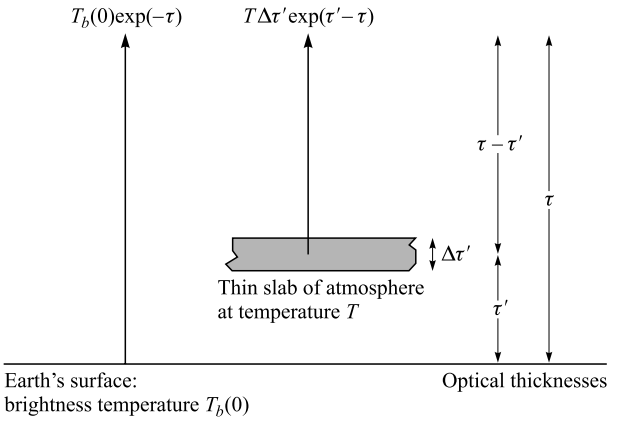

Figure 3.20. Contributions to the upward-propagating brightness temperature of the atmosphere. Heights above the Earth's surface are measured using the optical thickness τ.

[5] A much fuller treatment of the material presented in this section is given by Van de Hulst (1957, 1981). Useful material is also provided by Schanda (1986).

molecules to chapter 4, in which we consider propagation of radiation through the atmosphere.

A useful concept in understanding absorption and scattering by particles is the polarisability, which we have already met in section 3.1.1 and which will again be denoted by the symbol α. This is defined such that the dipole moment p induced in the particle when it is placed in an electric field E is given by αE. The direction of the dipole moment is the same as that of the electric field vector, but in an oscillating electric field, such as we will have in the case of electromagnetic radiation, the dipole moment might not be in phase with the electric field. For this reason, the polarisability α will in general be complex.

First, we will consider the absorption of electromagnetic energy by the particle. If the induced dipole moment p is varying with time, the instantaneous rate of power dissipation is given by $E\ dp/dt$. Putting

$$E = E_0 \exp(i\omega t)$$

for the electric field in the vicinity of the particle, we see that the dipole moment must be given by

$$p = \alpha E_0 \exp(i\omega t)$$

However, we recall that the physical meaning of these complex exponential expressions is contained in their real parts. We can assume that E_0 is real without any loss of generality, so we can rewrite our expression for E as

$$E = E_0 \cos(\omega t)$$

and obtain the following expression for dp/dt:

$$\frac{dp}{dt} = -\mathrm{Re}(\alpha)\omega E_0 \sin(\omega t) - \mathrm{Im}(\alpha)\omega E_0 \cos(\omega t)$$

The time-average of the dissipated power can then be obtained by multiplying these two expressions together, and averaging the result over time. This gives the mean dissipated power as

$$\langle P \rangle = -\frac{\omega \mathrm{Im}(\alpha)}{2} E_0^2$$

At this point, we can introduce the *absorption cross-section*, which we denote by the symbol σ_a. It is defined such that, if electromagnetic radiation of flux density F is incident on the particle, the mean absorbed power is given by

$$\langle P \rangle = \sigma_a F$$

Using equations (2.4), (2.7) and (2.8), we find that the absorption cross-section is given by

$$\sigma_a = -\frac{k}{\varepsilon_0} \mathrm{Im}(\alpha) \tag{3.75}$$

where k is the wavenumber of the radiation. It is clear that σ_a has the dimensions of an area, and this area has a physical interpretation: it is as though the particle absorbs all of the radiation incident within this cross-sectional area.

We can also note from equation (3.75) that the imaginary part of the polarisability cannot be negative.

For a small spherical particle of radius a and refractive index n (which may be complex), the polarisability is given by

$$\alpha = 4\pi\varepsilon_0 a^3 \left(\frac{n^2-1}{n^2+2}\right) \tag{3.76}$$

so the ratio of the absorption cross-section to the geometrical cross-section (πa^2) is

$$-\frac{8\pi a}{\lambda}\,\mathrm{Im}\left(\frac{n^2-1}{n^2+2}\right)$$

Because of our assumption that the radius a of the particle is much smaller than the wavelength λ, this expression will almost always be much smaller than 1. Thus, in the small-particle limit, the particle will absorb much *less* power than the power carried by a cross-section of the radiation equal to the geometrical area of the particle.

Next, we consider scattering by our small ($\ll \lambda$) particle. Classical electrodynamics shows that an oscillating electric dipole whose strength is described by

$$p = p_0 \sin(\omega t)$$

radiates a mean power of

$$\langle P\rangle = \frac{\mu_0 \omega^4 p_0^2}{12\pi c}$$

so the time-average of the power reradiated by a particle of polarisability α in an electromagnetic wave whose electric field vector is given by

$$E = E_0 \exp(i\omega t)$$

must be

$$\langle P\rangle = \frac{\mu_0 \omega^4 E_0^2}{12\pi c}\,|\alpha|^2$$

We can define the *scattering cross-section* σ_s in a manner similar to the absorption cross-section, such that the scattered power is $\sigma_s F$ when the particle is illuminated by radiation of flux density F. Again using equations (2.4), (2.7) and (2.8), we obtain the result

$$\sigma_s = \frac{k^4}{6\pi\varepsilon_0^2}\,|\alpha|^2 \tag{3.77}$$

As for the absorption cross-section, the scattering cross-section is much smaller than the geometrical cross-section of the particle, provided that the particle is small compared with the wavelength of the radiation.

We noted in section 3.4.1 that, in considering the scattering of radiation, we need to know how much energy is scattered in different directions. Equation (3.65) introduced the phase function as a means of specifying this. For the small-particle scattering described by equation (3.77), the phase function is given by

$$p(\cos\,\Theta) = \frac{3}{2}\left(1 - \cos^2\,\Theta\right) \tag{3.78}$$

(Note that the p in this expression is *not* the electric dipole moment!) Equation (3.78) shows that the scattering is maximum in the forward ($\Theta = 0$) and backward ($\Theta = \pi$) directions, and zero for scattering through $\pi/2$. The factor of $3/2$ ensures that the expression is correctly normalised, so that the integral over all directions is equal to 4π. For comparison, the phase function for an isotropic scatterer would be 1 in all directions.

Equations (3.75), (3.77) and (3.78) apply only to particles that are very small compared with the wavelength of the radiation. In this case, the scattering is often referred to as *Rayleigh scattering*. For larger particles, the situation becomes more complicated. If the particles are spherical with radius a, the problem can sometimes be analysed in terms of the dimensionless variable

$$x = \frac{2\pi a}{\lambda}$$

Rayleigh scattering then corresponds to the case when x is very small. The term *Mie scattering* is used to describe the situation for larger values of x. The extinction (attenuation) and scattering cross-sections can be expressed as

$$\frac{\sigma_e}{\pi a^2} = \frac{2}{x^2}\sum_{l=1}^{\infty}(2l+1)\left(\left|a_l^2\right| + \left|b_l^2\right|\right) \tag{3.79}$$

$$\frac{\sigma_s}{\pi a^2} = \frac{2}{x^2}\sum_{l=1}^{\infty}(2l+1)\mathrm{Re}(a_l + b_l) \tag{3.80}$$

where a_l and b_l, which are the *Mie coefficients*, depend on the complex refractive index and on the value of x. Equations (3.79) and (3.80) can be written as power series in x, in which case the first few terms are

$$\frac{\sigma_e}{\pi a^2} = -\mathrm{Im}\left\{4x\frac{n^2-1}{n^2+2} + \frac{4}{15}x^3\left(\frac{n^2-1}{n^2+2}\right)^2\frac{n^4+27n^2+38}{2n^2+3}\right\} + x^4\mathrm{Re}\left\{\frac{8}{3}\left(\frac{n^2-1}{n^2+2}\right)^2\right\} + \cdots \tag{3.81}$$

and

$$\frac{\sigma_s}{\pi a^2} = \frac{8}{3}\left|\frac{n^2-1}{n^2+2}\right|^2 x^4 + \frac{16}{45}\left|\frac{(n^2-1)^2(n^2-2)}{(n^2+2)^3}\right|x^6 + \frac{32}{27}\left|\frac{n^2-1}{n^2+2}\right|^3 x^7 + \cdots \tag{3.82}$$

We can recognise the first term in equation (3.81) as the result we have already derived for the absorption cross-section of a very small sphere, and the first term in equation (3.82) as the Rayleigh scattering cross-section. A simple iterative procedure for calculating the Mie coefficients, suitable for computing, has been presented by Deirmendjian (1969, pp. 14–15) and restated by Ulaby et al. (1981, volume 1, pp. 290–291).

Figure 3.21 shows the dependence of the ratios $(\sigma_e/\pi a^2)$ and $(\sigma_s/\pi a^2)$ calculated as a function of x for a refractive index $n = 5.67 - 2.88i$. For small values of x (the Rayleigh scattering region), the scattering cross-section is proportional to x^4, and the absorption cross-section is proportional to x. Since the absorption cross-section is much larger than the scattering cross-section, the absorption cross-section is also proportional to x. The figure also shows that, when x increases beyond about 1, the cross-sections pass through a maximum value that is of the order of the geometric cross-section, and then tend towards a constant value, usually with some oscillations. The grey lines in figure 3.21 show the asymptotic behaviour at small values of x. For the scattering cross-section, only the Rayleigh formula is shown since this provides an adequate approximation for values of x up to about 1. For the attenuation cross-section, the grey lines show the full expression of equation (3.81) (curve) and just its first term (straight line).

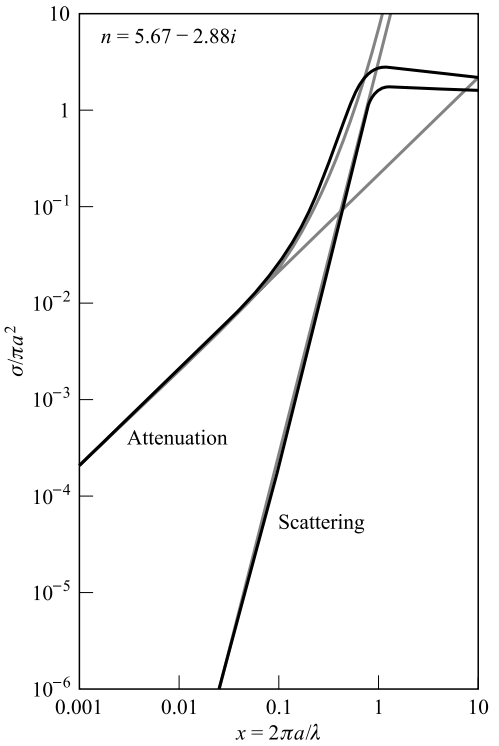

Figure 3.21. Dependence of the attenuation (extinction) and scattering cross-sections on the parameter x for a spherical particle of refractive index $n = 5.67 - 2.88i$. The grey curves show the asymptotic behaviour at small values of x.

Finally, we need to examine how the absorption and scattering cross-sections, which are defined for single particles, are related to the absorption and scattering coefficients. We will consider a thin slab of material, having cross-sectional area A and thickness Δz, with radiation of flux density F incident normally upon it. The material contains N particles per unit volume, each of which has absorption cross-section σ_a and scattering cross-section σ_s. It is clear that the slab must contain $NA\,\Delta z$ particles, so the total power that is absorbed by them is given by $F\sigma_a NA\,\Delta z$, provided that Δz is small enough. The flux density is thus reduced by $F\sigma_a N\,\Delta z$, so from equation (3.60) we can see that the absorption coefficient is

$$\gamma_a = N\sigma_a \tag{3.83}$$

A similar argument for scattering leads to the result that

$$\gamma_s = N\sigma_s \tag{3.84}$$

As an example, let us consider absorption and scattering of 1-cm microwaves by water droplets. We will take two hypothetical but fairly realistic cases: a cumulus cloud, in which the typical droplet radius $a = 2 \times 10^{-5}\,\mathrm{m}$ and the number density $N = 2 \times 10^{7}\,\mathrm{m}^{-3}$; and a light rainfall, for which $a = 1\,\mathrm{mm}$ and $N = 100\,\mathrm{m}^{-3}$. At a wavelength of 1 cm, the refractive index n of water is $5.67 - 2.88i$, so for the cloud droplets, for which $x = 0.0126$, equation (3.81) gives $\sigma_e = 3.58 \times 10^{-12}\,\mathrm{m}^2$ and equation (3.82) gives $\sigma_s = 7.73 \times 10^{-17}\,\mathrm{m}^2$. (In fact, just taking the first terms of the equations will give these values with sufficient accuracy.) The absorption cross-section is given by $\sigma_a = \sigma_e - \sigma_s$ as $3.58 \times 10^{-12}\,\mathrm{m}^2$. Multiplying these cross-sections by the number density of the droplets, we find that the scattering coefficient for cloud is $1.55 \times 10^{-9}\,\mathrm{m}^{-1}$, and the absorption and attenuation coefficients are $7.16 \times 10^{-4}\,\mathrm{m}^{-1}$ (approximately $0.3\,\mathrm{dB/km}$ [6]).

For the rain droplets $x = 0.63$. This is rather too large for equation (3.81) to give an accurate value for the attenuation cross-section, which is $4.78 \times 10^{-6}\,\mathrm{m}^2$, but equation (3.82) gives a reasonable estimate of the scattering cross-section as $1.40 \times 10^{-6}\,\mathrm{m}^2$ (the true value is $1.76 \times 10^{-6}\,\mathrm{m}^2$). The absorption cross-section is thus $3.02 \times 10^{-6}\,\mathrm{m}^2$, and the corresponding coefficients are as follows: scattering, $1.76 \times 10^{-4}\,\mathrm{m}^{-1}$ ($0.8\,\mathrm{dB\,km}^{-1}$); absorption, $3.02 \times 10^{-4}\,\mathrm{m}^{-1}$ ($1.3\,\mathrm{dBkm}^{-1}$); and attenuation, $4.78 \times 10^{-4}\,\mathrm{m}^{-1}$ ($2.1\,\mathrm{dB\,km}^{-1}$). Here, scattering, although still smaller than absorption, occurs at a significant level, and this illustrates the possibility of monitoring rainfall from ground-based *rain radars*.

[6] If the intensity of radiation (or anything else) is reduced by a factor x, this can equivalently be expressed as an attenuation by $10\,\log_{10}(x)$ decibels (dB). Thus, for example, an absorption coefficient of $y\,\mathrm{m}^{-1}$ can also be expressed as $10\,\log_{10}(e)\,y \approx 4.34\,y\,\mathrm{dB\,m}^{-1}$.

3.4.3 Simple models of volume scattering

It should be quite clear from the previous sections that volume scattering is a mathematically complicated phenomenon, and that no single model can embrace the range of possibilities that may occur. In this section, therefore, we will describe just one practical model of volume scattering. This was originally derived for the microwave backscatter from a snowpack, and is based on the work of Stiles and Ulaby (1980).

Figure 3.22 shows the situation schematically. Radiation is incident on the snowpack at an angle θ to the normal, and a fraction $T(\theta)$ of the incident power is transmitted across the interface, where

$$T(\theta) = |t(\theta)|^2$$

and $t(\theta)$ is the appropriate Fresnel coefficient (equation (3.31.2) or (3.31.4)). This radiation is refracted towards the normal at an angle θ', calculated from Snell's law (equation (3.30)).

Once inside the snowpack, the radiation undergoes volume scattering. In deriving equation (3.63), we saw that the power reflected out of an infinite volume-scattering medium in a simple one-dimensional model depended only on the ratio $\gamma_s/\gamma_a = \sigma_s/\sigma_a$. Plausibly, we may write the power backscattered from an infinite three-dimensional medium as

$$\frac{\gamma_s \cos\ \theta'}{2\gamma_e} = \frac{\sigma_s \cos\ \theta'}{2\sigma_e}$$

where the factor $(\cos\ \theta')/2$ has been introduced to account for the fraction of the total scattered power that is directed in the backscattering direction. However, the medium is not infinite, but instead has a depth d. The optical thickness of the path from the snow surface to the ground beneath is given by

$$\tau(\theta') = \gamma_e\ d\ \sec\ \theta'$$

and the fraction of power remaining after traversing this path twice (once in each direction) is $\exp(-2\tau(\theta'))$. If this fraction is zero, the medium is effectively infinitely deep so that volume scattering will contribute fully, whereas if it is 1

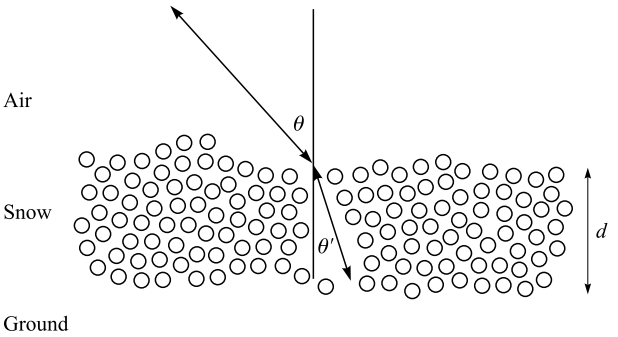

Figure 3.22. Volume scattering of microwave radiation from a snowpack (schematic).

the medium is transparent and volume scattering will not contribute at all. Thus, we may plausibly write

$$\frac{\gamma_s \cos\theta'}{2\gamma_e}(1 - \exp(-2\tau(\theta')))$$

for the fraction of the power entering the snowpack that is volume-scattered back to the surface. This radiation must again be transmitted through the snow–air interface, so our expression for the volume-scattering component of the backscatter coefficient becomes

$$T^2(\theta)\frac{\gamma_s \cos\theta'}{2\gamma_e}(1 - \exp(-2\tau(\theta')))$$

To complete the model, we need also to consider the surface scattering component and the component that is scattered from the snow–ground interface. We can write the latter term as

$$T^2(\theta)\sigma^0_{\text{ground}} \exp(-2\tau(\theta'))$$

to take into account that this radiation must pass through the air–snow interface twice and must also traverse the optical thickness $\tau(\theta')$ twice, so our final formula becomes

$$\sigma^0(\theta) = T^2(\theta)\left(\frac{\sigma_s \cos\theta'}{2\sigma_e}(1 - \exp(-2\tau(\theta'))) + \sigma^0_{\text{ground}} \exp(-2\tau(\theta'))\right) + \sigma^0_{\text{surface}}(\theta) \tag{3.85}$$

It should be emphasised that this is in fact a very simple volume-scattering model that does not take account of, amongst other things, multiple scattering. Nevertheless, it illustrates the principal considerations involved in such models.

3.5 Reflection and emission from real materials

We have now considered the factors that govern the reflection of electromagnetic radiation from solid and liquid surfaces in some detail, and we ought now to try to use these ideas to understand the reflectance properties of some real materials. By extension, we can also consider the emission properties in those parts of the electromagnetic spectrum – namely, the thermal infrared and microwave regions – in which they are important. The treatment in this section is rather brief. A fuller discussion can be found in, for example, Elachi (1987).

3.5.1 Visible and near-infrared region

The visible and near-infrared (VIR) region of the electromagnetic spectrum, from 0.4 μm to about 2 μm, is still the most important for remote sensing of the Earth's surface. The majority of remote sensing systems (with the exception of those designed to probe the Earth's atmosphere) operate in this region, and the data are intelligible to comparatively unskilled users.

Minor but significant use is still made of broad-band optical data, in which the reflected radiation is integrated over the whole of the visible part of the spectrum. This is, for example, roughly what is achieved by black-and-white (panchromatic) photography, and it is clear that what is measured is the spectrally averaged albedo. Figure 3.23 illustrates typical values of the albedo of various materials.

The lowest albedos are usually shown by water surfaces. The refractive index of water for visible light is roughly 1.33, so for normally incident radiation the Fresnel coefficient is given by equations (3.33.1) or (3.33.2) as 0.14 for the amplitude, and hence 0.02 for the intensity. The low albedo of pure water can therefore be explained in terms of the fact that the refractive index of water is not very different from 1. For 'real', naturally occurring, water, the albedo can be somewhat higher as a result of scattering by suspended particulate matter, or lower because of absorption. The refractive index of pure ice is similar to that of water, but naturally occurring ice generally contains a significant number density of trapped air bubbles that give rise to volume scattering, and hence a higher albedo.

The albedos of clouds (which are composed of small water droplets or ice crystals) and snow (a mixture of ice crystals, air and, in the case of wet snow, liquid water) are dominated by volume-scattering effects. We showed in section 3.4 that the extent of volume reflectance is governed by the ratio γ_s/γ_a. If we again consider a cumulus cloud in which the droplet radius $a = 2 \times 10^{-5}$ m, we see that the particle size parameter $x = 2\pi a/\lambda$ must be very large (several hundred) at optical wavelengths, so we expect the scattering cross-section to be of the order of πa^2. Taking the number density of the droplets to be $N = 2 \times 10^7\,\mathrm{m}^{-3}$, we therefore find the scattering coefficient to be of the order of $0.02\,\mathrm{m}^{-1}$. How can we estimate the absorption coefficient? Figure 3.1 shows that the absorption coefficient of pure water is of the order of

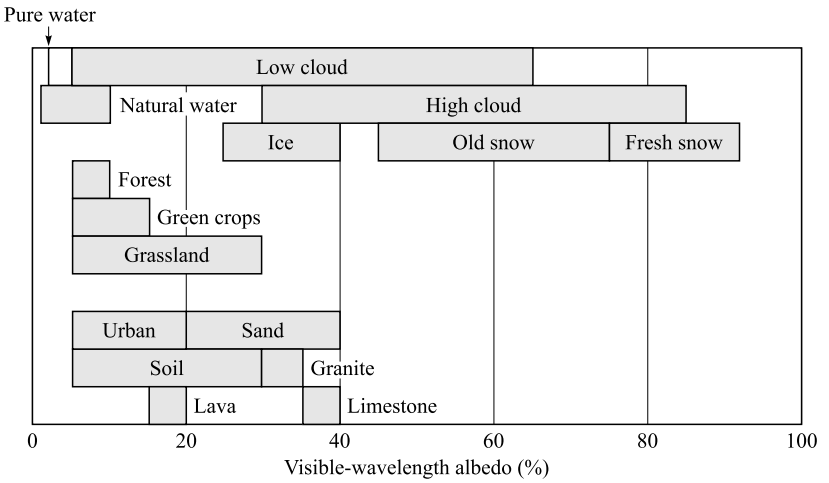

Figure 3.23. Typical values of albedo integrated over the visible waveband for normally incident radiation. (Mostly after Schanda, 1986.)

$0.01\,\mathrm{m}^{-1}$. However, one cubic metre of cloud contains only $4\pi a^3 N/3 = 7 \times 10^{-7}\,\mathrm{m}^3$ of water, so the average absorption coefficient of the cloud is roughly $10^{-8}\,\mathrm{m}^{-1}$. Thus, $\gamma_s/\gamma_a \approx 4 \times 10^6$, and we expect virtually all the radiation that enters the cloud to be scattered out of it, provided that it is optically thick. Since the attenuation length is of the order of 50 m, this condition is easily satisfied. A similar argument applies to snow.

Minerals, soils and the materials from which the visible parts of urban areas are composed show albedos typically in the range 5–40%. The dominant factor in these cases is the refractive index, since the scope for volume scattering is very limited. It is clear that the refractive index must be somewhat larger than that of water, typically between 1.6 and 4.5. If the materials are wet, the refractive index contrast between air and the material is reduced, and the reflectance is also reduced. Soils with a high content of organic material, which strongly absorbs light, also show low reflectance.

Finally, we consider the case of vegetation. Figure 3.23 shows quite low values of albedo for these materials in the optical region. This is again a consequence of absorption, by light-absorbing pigments (principally *chlorophyll* in the case of green vegetation), and is unsurprising since plants derive energy by absorbing light. However, figure 3.23 gives a very incomplete picture of the reflectance properties of vegetation in particular. To understand these better, we should examine the variation of reflectance with wavelength throughout the VIR region.

Figure 3.24 illustrates schematically the spectral reflectance (which we use as a general term to denote certain but unspecified conditions of illumination and viewing geometry) of various materials, in the wavelength range from 0.5 to 2.5 μm. The data are simplified, and fine detail has been omitted. Nevertheless, it is clear that in many cases the shape of such a curve (often called the *spectral*

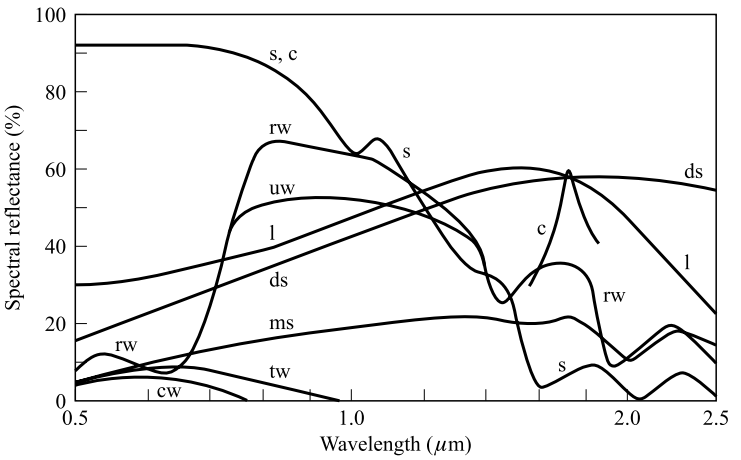

Figure 3.24. Typical spectral reflectances of various materials in the visible and near-infrared regions (schematic). s: snow; c: cloud; rw: ripe wheat; uw: unripe wheat; l: limestone; ds: dry soil; ms: moist soil; tw: turbid water; cw: clear water.

signature) is characteristic of the material, and indeed we are familiar with the idea that the colour of an object often gives a major clue to identifying it. The manner in which remotely sensed images with spectral content can be analysed to identify the probable distribution of materials represented within it will be discussed in chapter 11.

Let us comment on each of the spectral signatures of figure 3.24 in turn. In the case of water, there is little spectral structure, just a decline in reflectance at longer wavelengths as a result of increasing absorption. Limestone also exhibits little spectral structure (at the resolution of the figure), and dry loam broadly follows the same behaviour. However, moist loam exhibits a spectral reflectance that (a) is lower than that of dry loam, as we expect because of the reduced contrast in refractive index, and (b) shows a number of oscillations in the infrared part of the spectrum. These are due to *absorption lines* (absorption maximum near particular wavelengths) of water molecules. Much of this same absorption-line structure can also be seen in the spectral signature of snow.

Finally, we turn to the very characteristic spectral signature of vegetation (see also Curran, 1985), illustrated in figure 3.24 by the example of wheat. As we have remarked already, the low reflectance in the optical region is largely governed by the presence of pigments. The most important of these is chlorophyll, which has absorption maxima at 0.45 and 0.65 μm (respectively, blue and red), and consequently gives rise to a local maximum in the spectral reflectance at about 0.55 μm. This is the explanation for the green colour of much vegetable matter. The other important botanical pigments are carotene and xanthophyll (which give orange–yellow reflectance spectra) and the anthocyanins (red–violet). These latter pigments are dominant in the autumn, when the chlorophyll decomposes in many species, and give rise to the spectacular colours of autumn leaves (see Justice et al., 1985).

The high reflectance of vegetation in the near-infrared, roughly between 0.7 and 1.3 μm, is a volume-scattering effect. It is principally caused by multiple internal reflections of the radiation from hydrated cell walls in the *mesophyll* of the leaves, with little absorption. The transition from low reflectance in the red part of the spectrum to the much higher reflectance in the near-infrared is rather sharp, and is often termed the '*red edge*'. Above about 1.3 μm, the absorption of infrared radiation by water becomes significant (again we see the oscillatory structure that we noted for moist loam and for snow) and the reflectance is reduced. If the vegetation is stressed or diseased, the cell structure is less well developed or is damaged and the high reflectance between 0.7 and 1.3 μm is reduced. Stressed vegetation may also have a lower chlorophyll content than healthy vegetation, which will tend to increase the reflectance in the red part of the spectrum, so that the steepness of the red edge will be reduced. This phenomenon forms the basis of a number of techniques for assessing the amount and health of the vegetation present in a remotely sensed image, and will be discussed in more detail in chapter 11.

3.5.2 Emissivities in the thermal infrared region

The thermal infrared region was defined in chapter 2 as the range of wavelengths from 3 to 15 μm, and we saw in section 2.6 that objects at normal terrestrial temperatures radiate maximally in this part of the electromagnetic spectrum. The emissivity of a body (loosely speaking, its efficiency of emitting black-body radiation) at a given wavelength is negatively related to the reflectivity at the same wavelength, such that when the reflectivity is zero the emissivity is 1 and vice versa. For most naturally occurring materials, with the exception of metals and some minerals, the refractive index in the thermal infrared region is close to 1, which means that the reflectivity is low and the emissivity high. Figure 3.25 shows the emissivities of various materials. It should be noted that the emissivities shown in the figure are somewhat schematic, since the surface roughness of a material will also influence its emissiv-

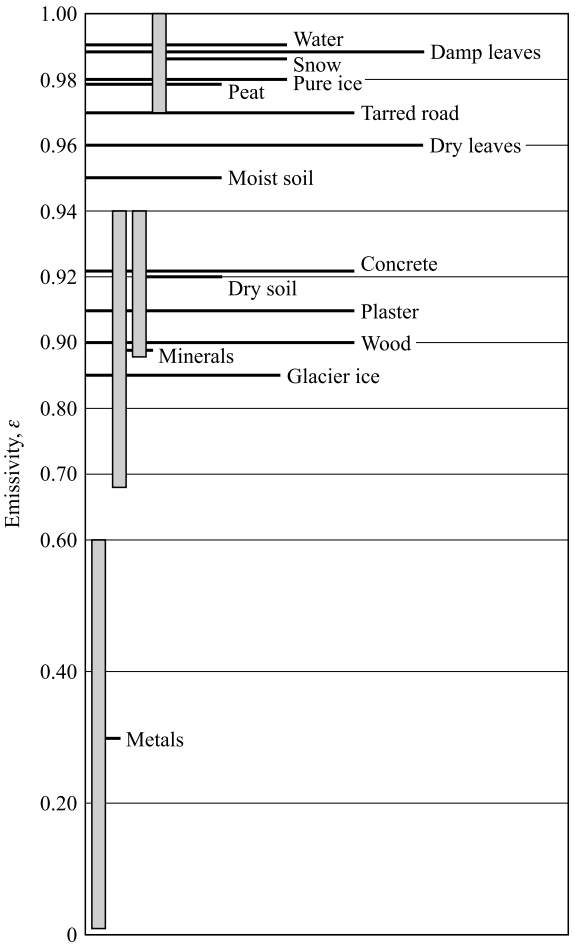

Figure 3.25. Typical emissivities of various materials at normal incidence in the range 8–12 μm. Note the change of scale at $\varepsilon = 0.90$.

ity. For example, a granite rock has a normal emissivity of about 0.89, but if the same material is highly polished, its emissivity will fall to about 0.80. In fact, the emissivity can be written generally in terms of the bidirectional reflectance distribution function (BRDF) as

$$\varepsilon_p = 1 - \int \left(R_{pp} + R_{qp}\right) \cos\theta_1 \, d\Omega_1 \tag{3.86}$$

where ε_p denotes the emissivity for p-polarised radiation and R_{qp} is the BRDF for radiation that is incident in the q-polarised state and reflected in the p-polarised state. θ_1 is the angle between the reflected radiation and the surface normal, and $d\Omega_1 = \sin\theta_1 \, d\theta_1 \, d\phi_1$ where ϕ_1 is the azimuth angle of the reflected radiation. The integration is carried out over 2π steradians; that is, $\theta_1 = 0$ to $\pi/2$ and $\phi_1 = 0$ to 2π. Emissivities can thus be calculated using equation (3.86) and the discussion of BRDFs presented in section 3.3.

3.5.3 Emissivities in the microwave region

Thermally generated radiation can also be detected in the microwave region of the electromagnetic spectrum; that is, at wavelengths between 1 mm and 1 m (frequencies between 0.3 and 300 GHz). As with thermal infrared emission, the physical parameter that determines the quantity of radiation that is emitted at a given temperature is the emissivity, and the principles that determine the emissivity are the same. In practical terms, however, the situation is more complicated than for thermal infrared emission. First, the range of wavelengths over which microwave observations can be made is much larger than for infrared observations. The latter are normally made in a single, rather broad, waveband from (typically) 8 to 12 μm, or perhaps in two narrower wavebands within this range, whereas microwave observations are routinely made at a number of frequencies spanning the range from (typically) 4 to 40 GHz – a factor of 10. It is therefore necessary to consider the variation of emissivity with frequency. Secondly, microwave observations are often made at angles away from the surface normal, so it is important to consider the dependence of the emissivity on the incidence direction.[7] Finally, the emissivities are often significantly different for different polarisation states, so that the dependence of polarisation must also be considered. These factors greatly increase the difficulty of providing a simple characterisation of the microwave emissivities of 'typical' materials. We will therefore content ourselves with illustrating the main features. A much fuller discussion is presented by Ulaby et al. (1982, volume 2).

For a homogeneous material (i.e. one in which volume-scattering effects are unimportant) with a smooth surface, the emissivity is given by $1 - |r|^2$, where r

[7] The widespread use of the term 'incidence direction' is potentially misleading, since we are discussing emitted, and not reflected, radiation, and perhaps a term such as 'outgoing direction' or 'viewing direction' would be more logical.

is the Fresnel reflection coefficient appropriate to the direction and polarisation of the radiation (this follows from equation (3.86)). Figure 3.26 illustrates this type of behaviour. The figure has been calculated using the Fresnel coefficients for a material with a dielectric constant of $18.5 - 31.3i$, which is appropriate for calm sea water at a temperature of 20°C and a frequency of 35 GHz. It can be noted from the figure that the emissivity for V- (vertically) polarised radiation increases to a maximum near 1 at about 80°. This is the phenomenon of the Brewster angle that we noted in section 3.2. The reason that the emissivity does not quite reach a value of 1 is because the dielectric constant is not real but complex. (We may also note in passing that the dielectric constant, and hence emissivity, of a water surface depends on temperature.)

Continuing with our example of sea water, we can consider the effect of varying the salinity. Increasing the salinity will increase the electrical conductivity of the water, and hence the Fresnel reflection coefficients, which will in turn lower the emissivity. However, we saw in figure 3.2 that the dielectric constant of sea water differs significantly from that of pure water only at frequencies below about 5 GHz, so we should not expect any significant dependence of emissivity on salinity above this frequency. We may also consider the effect of a rough surface, such as would be produced by wind action. This will lower the reflectance, and hence raise the emissivity, for observing directions away from the normal. Off-nadir observations of the microwave emission from a sea surface therefore have the potential to measure the sea state. The effect is greater at higher frequencies, which is consistent with the scattering models that we discussed in section 3.3.4, and is greater for horizontally than for vertically polarised radiation.

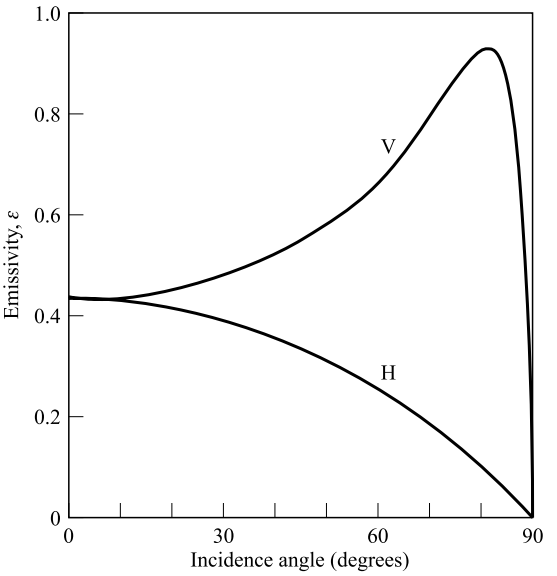

Figure 3.26. Emissivity of a material with a dielectric constant $18.5 - 31.3i$ as a function of incidence angle, for vertically and horizontally polarised radiation.

The microwave emissivity of a bare soil surface is dominated by the surface roughness and by the moisture content of the soil. The dielectric constant of water in the microwave region is much higher than that of soil (typically 3), so increasing moisture content will increase the reflectance and hence decrease the emissivity. Typical emissivities for soil surfaces lie in the range 0.5 to 0.95.

Volume-scattering effects are negligible in soils unless they are extremely dry. However, these effects can dominate in determining the emissivity properties of more open structures such as dry snowpacks and vegetation canopies. In such cases, the emissivity is given by

$$1 - \frac{\gamma_s}{\gamma_e}$$

for an optically thick medium in which multiple scatter is insignificant. Vegetation canopies have microwave emissivities typically in the range 0.85 to 0.99. A deep, dry snowpack has an emissivity of about 0.6. If the medium is not optically thick, the measured emission will include a contribution from the surface below, for example from the soil surface below a vegetation canopy. For a dry snowpack, the optical thickness at normal incidence is proportional to the total mass of ice per unit area of the pack, and this effect can therefore be used to estimate the snow mass. For wet snow, volume-scattering effects are insignificant and the emissivity is much higher, typically 0.95.

3.5.4 Microwave backscattering coefficients

From a practical point of view, it is as difficult to present characteristic data on the microwave backscattering properties of 'typical' materials as for their microwave emissivities. Again, the number of combinations of different observing parameters (frequency, polarisation and incidence angle) is very large, and the influence of natural variations in the physical properties of the scattering materials must also be taken into account. However, by way of example, figure 3.27 (which is mainly based on material presented by Long, 1983) illustrates the angular dependence of the backscattering coefficient σ^0 of a few representative materials at X-band. A much fuller discussion is presented by Ulaby et al. (1982, volume 2).

The backscatter from a concrete road surface is almost entirely due to surface scattering processes, and the low values of σ^0 at angles away from normal are consistent with a smooth surface, as expected. Surface scattering also dominates the backscatter from wet snow, the sea (in which case, the influence of wind speed on surface roughness is apparent), and urban areas. The dependence of the backscatter from a sea surface on the wind speed means that wind speed over the sea can be inferred from appropriate backscatter measurements (obviously, one would avoid incidence angles close to 10° where the sensitivity is very small). In fact, there is also a small dependence on wind *direction* (the data in figure 3.27c have been plotted for the case when the radar look direction

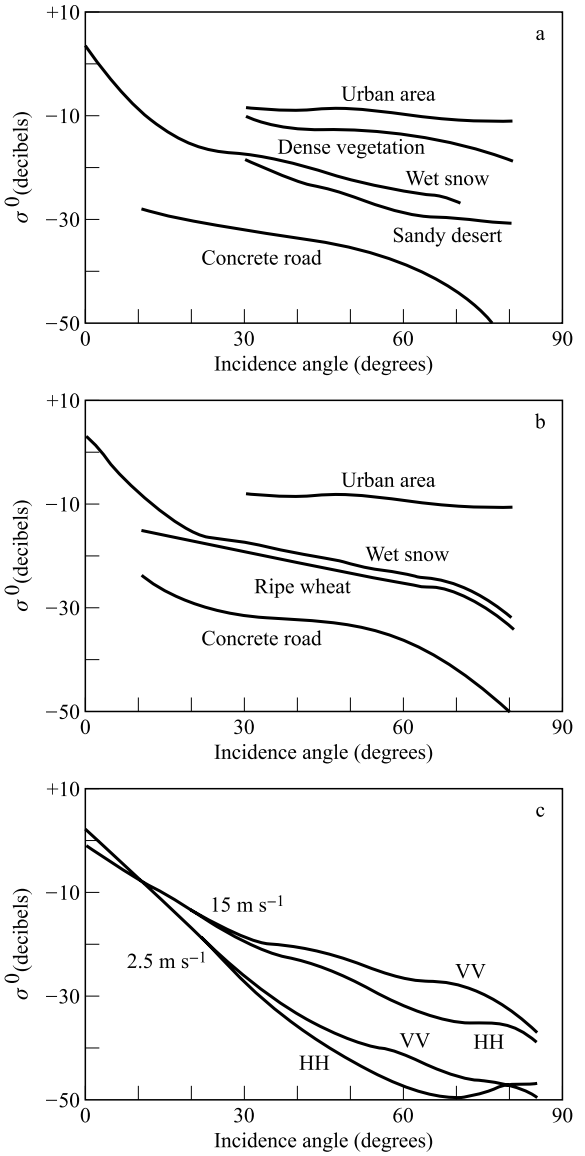

Figure 3.27. Representative X-band backscattering coefficients. (a) Various materials at HH-polarisation; (b) various materials at VV-polarisation; (c) sea surfaces at HH and VV polarisations. The curves have been labelled with the corresponding wind speed.

is upwind), which can be used to infer the wind velocity. The microwave backscattering properies of ocean surfaces are discussed further in section 9.4.1.

The high backscatter from urban areas, not strongly dependent on incidence angle, arises mainly from the presence of large numbers of planar surfaces, oriented at right angles to one another, in such areas. Figure 3.28 illustrates one of the mechanisms by which this occurs. If two reflecting planes are arranged perpendicularly (e.g. one plane could be the wall of a building and the other a road surface), incident radiation that strikes the concave region

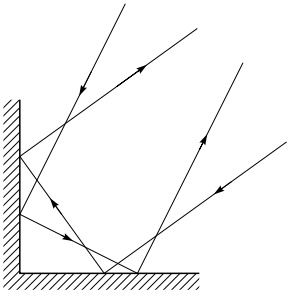

Figure 3.28. Radiation is reflected by two perpendicular planes so that it returns along the incidence direction. This is an important contributor to the strong microwave backscatter from urban areas.

between the planes from any direction in the plane that contains the normals to both surfaces will be reflected back along its incidence direction. In fact, if *three* planar surfaces meet at right angles, radiation from *any* direction that strikes the concave region between them will be scattered back along its incidence direction. Thus, a region that contains a large number of such 'inside corners' will give strong specular scattering from most incidence directions.

Dry deserts, vegetation canopies and dry snowpacks are examples of media from which volume-scattering effects are important. In general, the backscattering in such cases will show a weaker dependence on incidence angle than is observed in cases where surface scattering dominates. A dry desert can be assumed to be optically thick (physical depth much larger than the attenuation length). However, for dry snow and vegetation canopies, this assumption may not be true. For example, radiation incident close to vertically on an agricultural crop is likely to be scattered significantly from the soil below. In the case of dry snow, the assumption of optical thickness is often not valid since the attenuation depth may be many metres. Thus, a dry snow cover a few tens of centimetres deep may be practically invisible to microwave radiation.

The data presented in figure 3.27 show only the co-polarised (like-polarised) backscattering coefficients: namely HH and VV. In general, the cross-polarised components (HV and VH) are extremely small unless multiple volume-scattering occurs.

PROBLEMS

1. Show that the real and imaginary parts of the refractive index of a non-magnetic material are given by

$$m = \sqrt{\frac{\sqrt{\varepsilon'^2 + \varepsilon''^2} + \varepsilon'}{2}}$$

$$\kappa = \sqrt{\frac{\sqrt{\varepsilon'^2 + \varepsilon''^2} - \varepsilon'}{2}}$$

2. A commonly used approximation to the absorption length is

$$l_a \approx \frac{\sqrt{\varepsilon'}}{2\pi\varepsilon''}\lambda_0$$

where λ_0 is the free-space wavelength. Show that this approximation is accurate to within 1% if $\varepsilon''/\varepsilon' < 0.28$.

3. Sea water has an electrical conductivity σ of typically about 4 S m^{-1}. The real part of its dielectric constant at radio frequencies of 100 MHz and below is 88.2. By assuming that the imaginary part is given by equation (3.23), find the absorption length of electromagnetic waves at 100 MHz and 100 kHz.

4. Randomly polarised radiation at a wavelength of 3 cm is incident on a plane water surface at an angle of 83° to the normal. Calculate the Stokes vector, and hence polarisation state, of the reflected radiation. The dielectric constant of water at 3 cm is $63.1 - 32.1i$.

5. (For mathematical enthusiasts.) Show that the diffuse albedo for specular reflection of perpendicularly polarised radiation is

$$\frac{3n^2 - 2n - 1}{3(n+1)^2}$$

and confirm that this expression has the correct limiting forms as the refractive index n tends to 1 and to infinity.

6. A rough surface has a BRDF proportional to $\cos(\theta_0)\cos(\theta_1)$, where θ_0 and θ_1 are, respectively, the angles of the incident and scattered radiation measured from the surface normal. The BRDF has no azimuthal dependence. Show that, if the albedo for normally incident radiation is 1, the diffuse albedo of the surface is 2/3.

7. Consider scattering from a surface with r.m.s. height variation $= \lambda/2$, where λ is the wavelength. Show that the stationary phase model can describe this scattering provided that the incidence angle is less than about 60° and $m < 0.60$, whereas the scalar model requires $m < 0.25$, where m is the r.m.s. surface slope variation.

8. Prove equation (3.63).

9. A typical pack of freshly fallen snow has a density of 100 kg m^{-3} and consists of ice crystals which can be modelled as spheres of radius 0.5 mm. Show that if the snowpack is sufficiently deep it would be expected to have a visible-band albedo close to 1, and estimate the depth necessary for this to occur. The absorption coefficient for light in ice can be taken as 0.01 m^{-1}, and the density of pure ice is 920 kg m^{-3}.